Author Manuscript

Author Manuscript

Author Manuscript

Author Manuscript

HHS Public Access

Author manuscript

Nature. Author manuscript; available in PMC 2018 December 20.

Published in final edited form as:

Nature. 2018 August ; 560(7718): 387–391. doi:10.1038/s41586-018-0290-0.

A Multiprotein Supercomplex Controlling Oncogenic Signaling in Lymphoma

James D. Phelan[#1], **Ryan M. Young**[#1], **Daniel E. Webster**[1], **Sandrine Roulland**[1,18], **George W. Wright**[2], **Monica Kasbekar**[1], **Arthur L. Shaffer III**[1], **Michele Ceribelli**[3], **James Q. Wang**[1], **Roland Schmitz**[1], **Masao Nakagawa**[1], **Emmanuel Bachy**[1], **Da Wei Huang**[1], **Yanlong Ji**[4], **Lu Chen**[3], **Yandan Yang**[1], **Hong Zhao**[1], **Xin Yu**[1], **Weihong Xu**[1], **Maryknoll M. Palisoc**[5], **Racquel R. Valadez**[5], **Theresa Davies-Hill**[5], **Wyndham H. Wilson**[1], **Wing C. Chan**[6], **Elaine S. Jaffe**[5], **Randy D. Gascoyne**[7], **Elias Campo**[8], **Andreas Rosenwald**[9], **German Ott**[10], **Jan Delabie**[11], **Lisa M. Rimsza**[12], **Fausto J. Rodriguez**[13], **Fayez Estephan**[14], **Matthias Holdhoff**[14], **Michael J. Kruhlak**[15], **Stephen M. Hewitt**[16], **Craig J. Thomas**[1,3], **Stefania Pittaluga**[5], **Thomas Oellerich**[1,4,17,§], and **Louis M. Staudt**[1,§]

[1]Lymphoid Malignancies Branch, National Cancer Institute, National Institutes of Health, Bethesda, MD 20892

[2]Biometric Research Branch, Division of Cancer Diagnosis and Treatment, National Cancer Institute, National Institutes of Health, Bethesda, MD, USA

[3]Division of Preclinical Innovation, National Center for Advancing Translational Sciences, National Institutes of Health, Gaithersburg, MD 20850, USA

[4]Department of Medicine II, Hematology/Oncology, Goethe University, Theodor-Stern-Kai 7, 60590 Frankfurt, Germany

[5]Laboratory of Pathology, Center for Cancer Research, National Cancer Institute, National Institutes of Health, Bethesda, MD 20892

[6]Departments of Pathology, City of Hope National Medical Center, Duarte, CA 91010

[7]British Columbia Cancer Agency, Vancouver, British Columbia, Canada V5Z 4E6

[8]Hospital Clinic, University of Barcelona, 08036 Barcelona, Spain

[9]Institute of Pathology, University of Würzburg, and Comprehensive Cancer Center Mainfranken, 97080 Würzburg, Germany

Users may view, print, copy, and download text and data-mine the content in such documents, for the purposes of academic research, subject always to the full Conditions of use:http://www.nature.com/authors/editorial_policies/license.html#terms

§ These authors jointly supervised this work: Louis M. Staudt, M.D., Ph.D., lstaudt@mail.nih.gov, Thomas Oellerich, M.D., thomas.oellerich@kgu.de.

Author Contributions

JDP and RMY designed and performed experiments, analyzed data, made figures and wrote the manuscript. DEW, MJK and SP designed and performed experiments and analyzed data. SR, MK, ALSIII, MC, JQW, RS, MN and EB performed experiments and analyzed data. GWW, DWH, LC, and CJT analyzed data, YJ, YY, HZ, XY, WX, MMP, RRV, TD-H performed experiments, WHW, WCC, ESJ, RDG, EC, AR, GO, JD, LMR, FJR, FE, MH and SMH provided clinical samples. TO and LMS designed experiments, analyzed data, made figures and wrote the manuscript.

The authors state they have no competing interests.

Author Manuscript Author Manuscript Author Manuscript Author Manuscript

[10]Department of Clinical Pathology, Robert-Bosch-Krankenhaus, and Dr. Margarete Fischer-Bosch Institute for Clinical Pharmacology, 70376 Stuttgart, Germany

[11]University Health Network, Laboratory Medicine Program, Toronto General Hospital and University of Toronto, Toronto, ON, M5G 2C4, Canada

[12]Department of Laboratory Medicine and Pathology, Mayo Clinic, Scottsdale, AZ 85259

[13]Department of Pathology, Johns Hopkins University School of Medicine

[14]Department of Oncology, Sidney Kimmel Comprehensive Cancer Center at Johns Hopkins, Johns Hopkins University School of Medicine, Baltimore, MD 21287, USA

[15]Experimental Immunology Branch, National Cancer Institute, National Institutes of Health, Bethesda, MD 20892

[16]Experimental Pathology Laboratory, National Cancer Institute, National Institutes of Health, Bethesda, MD 20892

[17]German Cancer Research Center and German Cancer Consortium, 69120 Heidelberg, Germany

[18]Current address: Aix-Marseille university, CNRS, INSERM, Centre d'Immunologie de Marseille-Luminy, Marseille, France

[#] These authors contributed equally to this work.

Summary

B cell receptor (BCR) signaling has emerged as a therapeutic target in B cell lymphomas, but inhibiting this pathway in diffuse large B cell lymphoma (DLBCL) has benefited only a subset of patients[1]. Gene expression profiling identified two major DLBCL subtypes, known as germinal center (GC) B cell-like (GCB) and activated B cell-like (ABC)[2,3], with inferior outcomes following immunochemotherapy in ABC. Autoantigens drive BCR-dependent activation of NF-κB in ABC DLBCL through a kinase cascade of SYK, BTK and PKCβ to promote the assembly of the CARD11-BCL10-MALT1 (CBM) adapter complex that recruits and activates IκB kinase (IKK)[4,5,6]. Genome sequencing revealed gain-of-function mutations targeting the CD79A and CD79B BCR subunits and the Toll-like receptor (TLR) signaling adapter MYD88[5,7], with $MYD88^{L265P}$ being the most prevalent isoform. In a clinical trial, the BTK inhibitor, ibrutinib, produced responses in 37% of ABC cases[1]. The most striking response rate (80%) was observed in tumors with both *CD79B* and $MYD88^{L265P}$ mutations, but how these mutations cooperate to promote dependence on BCR signaling remains unclear. Herein, we used genome-wide CRISPR-Cas9 screening and functional proteomics to understand the molecular basis for exceptional clinical responses to ibrutinib. We discovered a new mode of oncogenic BCR signaling in ibrutinib-responsive cell lines and biopsies, coordinated by a multiprotein supercomplex formed by MYD88, TLR9, and the BCR (My-T-BCR). The My-T-BCR co-localizes with mTOR on endolysosomes, where it drives pro-survival NF-κB and mTOR signaling. Inhibitors of BCR and mTOR signaling cooperatively decreased My-T-BCR supercomplex formation and function, providing mechanistic insight into their synergistic toxicity for My-T-BCR^+ DLBCL cells. My-T-BCR complexes characterized ibrutinib-responsive malignancies and distinguished ibrutinib

Author Manuscript Author Manuscript Author Manuscript Author Manuscript

responders from non-responders. Our data provide a roadmap for the rational deployment of oncogenic signaling inhibitors in molecularly-defined subsets of DLBCL.

We used a library of small guide RNAs (sgRNAs) to conduct genome-wide loss-of-function CRISPR-Cas9 screens for essential genes in lymphoid cell lines engineered with inducible Cas9. We screened three ibrutinib-sensitive ABC lines, one ibrutinib-insensitive ABC line, and four ibrutinib-insensitive GCB lines, as well as two multiple myeloma and one T cell lymphoma line as controls (Extended data Fig. 1a, Table S1–S2). For each gene, we derived a gene-level statistic that we term a CRISPR screen score (CSS), which is, in essence, the number of standard deviations away from the average effect of inactivating a gene (Table S3, see Methods).

Control, non-targeting sgRNAs were not toxic, whereas sgRNAs targeting pan-essential genes[8] were depleted in all lines (Extended data Fig. 1b). Among genes encoding B-cell transcription factors, we observed DLBCL subtype-specific dependencies in both GCB (MEF2B, TCF3, IRF8, SPI1), and ABC lines (IRF4, SPIB, BATF) (Extended data Fig. 1c). Results from a validation screen using ~10 sgRNAs per gene (Tables S4–S5) were strongly correlated with those from the genome-wide screens ($p<0.0001$; Table S6, Extended data Fig. 2a).

Most DLBCL lines depended on the BCR subunits CD79A and CD79B (Fig. 1), but engaged divergent downstream survival pathways. ABC lines uniquely relied on NF-κB regulators and on JAK1/STAT3 signaling triggered by the NF-κB-dependent cytokine IL-10. By contrast, BCR signaling in GCB lines was NF-κB-independent, but shared a dependence on PI3K/mTOR signaling with ABC, albeit using different signaling adapters (PIK3AP1 in ABC, CD19 in GCB). The BCR signaling mode in GCB is akin to that observed in another GC-derived malignancy, Burkitt lymphoma[9], which was previously called “tonic signaling” because it resembled tonic, NF-κB-independent BCR signaling in naïve mouse B cells.[10] However, GCB and Burkitt lines depended on CD19 and LYN (Fig. 1, Extended data Fig. 3), which are not required for tonic signaling in mouse B cells, so we instead dub this phenomenon “constitutive GC BCR signaling”.

The survival of BCR-dependent ABC lines relied on TLR9, which coordinates MYD88 signaling in innate immune cells, and on two chaperones that regulate the subcellular localization of TLR9, CNPY3 and UNC93B1. TLR9 was the only essential TLR in ABC lines (Extended data Fig. 2b). We validated these findings using time-dependent toxicity assays in 12 DLBCL lines transduced with vectors co-expressing sgRNAs and GFP (Fig. 2a). As expected, ABC lines expressing mutant isoforms of MYD88 were sensitive to MYD88 deletion[7]. In contrast, TLR9, and its chaperones UNC93B1 and CNPY3 [11] were only essential in ABC lines with *MYD88*^{L265P} and either a *CD79B* or *CD79A* mutation. These “double-mutant” lines were also particularly sensitive to BTK inhibition (Table S1).

We next investigated copy number and gene expression levels of TLR pathway genes in 574 DLBCL tumors.[12] ABC tumors had recurrent single copy gains or amplifications involving *MYD88*, *TLR9*, *CNPY3,* and *UNC93B1*, all of which were more highly expressed in ABC tumors and their expression correlated with copy number (Fig. 2b, Extended data Fig. 4a,

Author Manuscript Author Manuscript Author Manuscript Author Manuscript

Table S7). Altogether, 49.7% of ABC tumors had increased copy number of one or more of these genes (Fig. 2b, Table S8), with *CNPY3* and *UNC93B1* demonstrating minimal common amplified regions of 1.1Mb and 277kb respectively (Extended data Fig. 4b, Table S9). These data provide genetic evidence that the TLR9 pathway contributes to the ABC phenotype.

To elucidate TLR9 function in ABC DLBCL, we expressed a fusion protein linking TLR9 to BioID2, a promiscuous biotin ligase that biotinylates proteins within ~10 nm[13]. Biotinylated proteins in TLR9-BioID2-expressing ABC cells were purified and compared to proteins from control cells by SILAC-based quantitative mass spectrometry (MS). To define the TLR9 interactome that is essential in ABC DLBCL, we compared the MS enrichment of each protein with its respective CSS metric (Fig. 2c). The TLR9-essential interactome confirmed association of TLR9 with MYD88 and CNPY3, but also revealed interactions with the BCR subunits CD79A and CD79B (Figs. 2c, Extended data 4c–e, Tables S10–11). The IgM component of the endogenous BCR co-immuneprecipitated with TLR9 in three ABC lines more than in a GCB line (Fig. 2d). By contrast, neither TLR4 nor TLR7 co-immunoprecipitated with IgM (Extended data Fig. 5a). TLR9 associated with IgM in an intracellular fraction of ABC cells rather than a plasma membrane fraction (Extended data Fig. 5b), suggesting that the BCR and TLR9 might cooperate at an intracellular location.

To visualize where TLR9 and the BCR interact, we employed proximity ligation assays (PLA), which identify proteins within tens of nanometers of each other[14]. An IgM:TLR9 PLA produced fluorescent puncta in the cytoplasm of ABC cells which was reduced by depletion of CD79A or TLR9 (Fig. 2e, Extended data Fig. 5c). IgM:TLR9 PLA signal was present across a panel of BCR-dependent ABC lines, with higher signals in double-mutant lines, whereas BCR-independent ABC and GCB lines had substantially lower signals (Extended data Fig. 5d–f). IgG:TLR9 PLA gave no detectable signal (Extended data Fig. 5g). IgM:TLR9 PLA signals co-localized with the endolysosomal marker LAMP1 (Extended data Fig. 5h–i), consistent with the dependence of these ABC lines on UNC93B1 and CNPY3, which facilitate TLR9 entry into $LAMP1^{+}$ endolysosomes.[11] Ectopic expression of TLR9, $MYD88^{WT}$ or $MYD88^{L265P}$ increased the IgM:TLR9 PLA signal (Extended data Fig. 5j), suggesting that TLR9/MYD88 copy number gains in ABC tumors augment BCR-TLR9 cooperation.

Knockdown of TLR9 decreased NF-κB-dependent gene expression and reduced IκB kinase activity in ABC lines with $MYD88^{L265P}$, confirming the role of TLR9 in oncogenic NF-κB signaling (Extended data Fig. 6). TLR9:MYD88 PLA puncta were visible in the cytoplasm of ABC lines, but were diminished by knockdown of TLR9, MYD88, or CD79A, suggesting that the BCR facilitates recruitment of MYD88 to TLR9 (Fig. 2f).

These results suggest that TLR9 coordinates signaling between the BCR and MYD88. We hypothesized that the BCR, TLR9 and MYD88 nucleate a signalosome that activates NF-κB, which we will term the MyD88-TLR9-BCR (My-T-BCR) supercomplex. To identify additional My-T-BCR components, we expressed a $MYD88^{L265P}$-BioID2 protein in three ABC lines and performed MS analysis of MYD88-proximal biotinylated proteins. We identified proteins biotinylated in all three lines and used their CSS scores to define the

Author Manuscript Author Manuscript Author Manuscript Author Manuscript

essential MYD88 interactome, which included the BCR (CD79B), mTOR, PLCγ2, and the CBM complex (CARD11, MALT1) (Fig. 3a, Extended data 7a–b, Table S12–14). Streptavidin pulldown and immunoblot analysis confirmed CARD11 and MALT1 biotinylation in ABC cells with MYD88^{L265P}-BioID2 (Extended data Fig. 7c–d).

Finding the CBM complex in proximity to MYD88 was unexpected since these adaptors are thought to independently promote NF-κB activation. Both MALT1:MYD88 and BCL10:MYD88 PLAs yielded robust cytoplasmic puncta in ABC cells, confirming the association of endogenous MYD88 with the CBM complex (Fig. 3b, Extended data 7e-f). These PLA signals were reduced by knockdown of CD79A, TLR9, and CARD11, suggesting that BCR and TLR9 signaling cooperate to assemble MYD88 and the CBM into a supercomplex. Moreover, CARD11:BCL10 PLA puncta were reduced by knockdown of TLR9 or MYD88 in double mutant cell lines, demonstrating that TLR9 signaling controls CBM complex assembly in ABC cells (Fig. 3d, Extended data 7g).

NF-κB is activated by IKK-dependent phosphorylation of IκBα. By PLA, both IgM and TLR9 associated with phospho-IκBα in the cytoplasm of ABC cells, which was reduced by knockdown of CD79A, TLR9 or MYD88 (Fig. 3d-e). Thus, NF-κB activation is closely associated with the My-T-BCR complex.

We next visualized the subcellular location of the My-T-BCR complex by staining ABC cells bearing MYD88^{L265P}-BioID2 with fluorescently-labeled streptavidin. The MYD88-BioID2 signal defined large cytoplasmic structures that co-localized with phospho-IKK, consistent with active NF-κB signaling at these sites (Fig. 3f; Supplementary video 1). These complexes extended into the cytoplasmic space from the surface of LAMP1^{+} vesicles. BCR was visualized by cell surface labelling of IgM with a fluorescent Fab on ice, followed by brief warming to allow internalization. The LAMP1^{+} vesicles with MYD88-BioID2 signals also contained IgM, suggesting a dynamic shuttling of the BCR from the plasma membrane to the intracellular site of My-T-BCR complex formation.

Given that the My-T-BCR complex coordinates pro-survival signaling in ABC DLBCL, we hypothesized that inhibition of BTK activity by ibrutinib might disrupt this signaling complex. Ibrutinib reduced My-T-BCR puncta in ABC lines bearing MYD88^{L265P}-BioID2 (Extended data Fig. 7h). To globally assess the effect of ibrutinib on the My-T-BCR, we treated two ABC lines bearing MYD88^{L265P}-BioID2 with ibrutinib and analyzed the biotinylated proteins by MS. Interactions of MYD88 with the CBM complex (CARD11), PLCγ2, and mTOR were disrupted by ibrutinib (Fig. 4a, Extended data 7i, Table S14–15).

The ibrutinib-sensitive association of mTOR with MYD88 suggested that signaling by the My-T-BCR complex might affect pathways controlled by mTOR. Of note, components of the Ragulator complex (LAMTOR1, LAMTOR3, LAMTOR4, RRAGA), which regulates mTORC1 activity at the lysosomal membrane[15], were biotinylated by TLR9-BioID2, as were components of the lysosomal V-ATPase (ATP6V1B2, ATP6V0D1), which regulates the mTORC1 response to amino acids[16] (Fig. 2c, Extended data 4C, Table S10–11). In ABC lines with MYD88^{L265P}-BioID2, mTOR localized to LAMP1^{+} vesicles, often in proximity to the My-T-BCR (Fig. 4b). PLA in three ABC lines confirmed that ibrutinib decreased

Author Manuscript Author Manuscript Author Manuscript Author Manuscript

association of endogenous MYD88 with mTOR, MALT1, and BCL10 (Fig. 4c). Ibrutinib also decreased the association of IgM and phospho-IκBα, but had mixed effects on IgM association with TLR9. These findings suggest that IgM trafficking to TLR9^{+} endolysosomes is constitutive, but interaction of the My-T-BCR complex with mTOR, the CBM complex, and NF-κB is controlled by BTK-dependent BCR signaling.

Given the proximity of MYD88 and mTOR, we investigated the effect of mTOR inhibition on the My-T-BCR. In MYD88^{L265P}-BioID2-expressing ABC cells, My-T-BCR formation was reduced by ibrutinib, but was further attenuated by the addition of AZD2014, an mTORC1/2 inhibitor (Fig. 4d). Dual mTOR and BTK inhibition cooperatively decreased MYD88 protein levels and blocked mTOR activity, as assessed by phospho-4E-BP1 and phospho-S6 kinase, as well as NF-κB activation, as assessed by phospho-IKK (Fig. 4e). These data provide mechanistic insights into the synergism between BTK inhibitors and drugs targeting mTOR or PI3K in ABC models growing in vitro (Fig. 4f) and in vivo (Fig. 4g).[17,18]

Finally, we examined whether the My-T-BCR complex is detectable in primary lymphoma biopsy samples, and if its presence might be associated with ibrutinib responsiveness. We optimized the PLA for use in formalin-fixed biopsy samples using a tissue microarray of 81 lymphoma cell lines. IgM:TLR9 PLA signals were highest in ABC lines with chronic active BCR signaling, with little if any PLA signal in other lymphoma lines or normal B cells present in tonsils or reactive lymph nodes (Extended data Fig. 8a–b, Table S17). Among DLBCL biopsies, ABC cases had significantly more IgM:TLR9 puncta than GCB cases (Fig. 5a). High IgM:TLR9 PLA signals were also observed in biopsies of primary central nervous system lymphoma (PCNSL), Waldenström macroglobulinemia (WM), and its relative, lymphoplasmacytic lymphoma (LPL) (Fig. 5b). These malignancies commonly have *MYD88*^{L265P} and/or *CD79A* or *CD79B* mutations, and respond frequently to ibrutinib[19–23]. Of two WM lines tested, one had My-T-BCR complexes, and knockdown of the BCR (CD79A) or TLR9 was selectively toxic for this line (Extended data Fig. 9a–c). My-T-BCR complexes were not evident in mantle cell lymphoma (MCL) or chronic lymphocytic leukemia (CLL) samples (Fig. 5b), suggesting that these malignancies rely on a qualitatively distinct form of BCR signaling.

We next examined eight available biopsies from patients with relapsed or refractory DLBCL enrolled on a clinical trial of ibrutinib monotherapy[1]. We adapted the IgM:TLR9 PLA to allow immunohistochemical identification of CD20^{+} lymphoma cells (Fig. 5c). Three ABC cases and one unclassified DLBCL scored positive in the IgM:TLR9 PLA while three other ABC cases and one GCB case were negative (see Methods; Table S16). The percentage of IgM:TLR9 PLA-positive malignant cells was significantly higher in tumors that responded to ibrutinib than in those that progressed on treatment (Fig. 5d). In this series, two responding cases with IgM:TLR9 puncta had *CD79B* or *CD79A* mutations, respectively, but lacked MYD88^{L265P}, while two other responders were wild-type for these genes (Table S16). These findings demonstrate that the My-T-BCR exists in ABC DLBCL tumors that respond to ibrutinib, even in those lacking the *MYD88*^{L265P}/*CD79B* double-mutant genotype.

Author Manuscript Author Manuscript Author Manuscript Author Manuscript

We provide genetic, proteomic, cell biological and functional evidence for a novel, pro-survival signaling hub – termed the My-T-BCR supercomplex – that coordinates NF-κB activation in DLBCL and identifies tumors that respond to therapeutic inhibition of NF-κB by ibrutinib. This supercomplex is present in a subset of ABC DLBCL lines and tumors, but is generally absent from GCB DLBCL, which have an alternative "constitutive GC" BCR signaling mode, requiring distinct therapeutic strategies (Fig. 5e). The My-T-BCR supercomplex provides mechanistic insight into the efficacy of drug combinations in ABC DLBCL and may aid in the development of predictive assays to identify patients who would benefit from drugs targeting BCR-dependent NF-κB activation, including BTK inhibitors.

Methods

Cell culture

Cell lines were grown at 37°C in the presence of 5% CO_2 and maintained in RPMI supplemented with fetal bovine serum (Tet tested, Atlanta Biologics,) and 1% pen/strep and 1% L-glutamine (Invitrogen), except for OCI-Ly10 and OCI-Ly3 which were grown in IMDM supplemented with 20% heparinized human plasma, 1% pen/strep and 55uM β-mercaptoethanol. All cell lines were regularly tested for mycoplasma using the MycoAlert Mycoplasma Detection Kit (Lonza) and DNA fingerprinted by examining 16 regions of copy number variants (Jonathan Keats, personal communication). OCI-LY3, although present database of commonly misidentified cell lines maintained by ICLAC, was included in this study as a necessary model of a BCR-independent, *MYD88*^{L265P} mutant, MYD88-dependent ABC DLBCL. This cell line was authenticated by DNA fingerprinting and compared to historical DNA controls.

Cas9 vector construction

pRetroCMV/TO-Cas9-Hygro was created by ligating the tetracycline-inducible CMV promoter from pcDNA4/TO (Invitrogen) with MfeI/XbaI and blunt cloned into the XhoI/EcoRI digested pRetrosuper vector [24]. The puromycin resistance gene from pRetroCMV/TO was removed with StuI/ClaI and replaced with PGK-hygromycin which was isolated from pMSCV Hygro (Clonetech) with AgeI/HindIII and similarly cloned into pRetroCMV/TO. Cas9 was isolated from the LentiCrispr v2 (Addgene #52961) and blunt cloned into pRetroCMV/TO-hygro digested with AgeI/BamHI. pCW-Cas9-Blasticidin was generated from pCW-Cas9-puro which was purchased from Addgene (#50661) and digested with BamHI and XbaI to remove the puromycin resistance gene. A g-block (IDT) containing the blasticidin resistance gene was Gibson cloned into the cut vector with 12 basepair overlaps.

Cas9-clone generation

Cell lines were transduced multiple times with either pTO-Cas9-hygro or pCW-Cas9, selected and dilution cloned. Single cell clones were picked and tested for functional Cas9 cutting after transduction with sgRNAs targeting surface markers including CD20 or ICAM1. Clones were selected based upon loss of surface expression within the transduced population as measured by FACS 8–14 days after addition of doxycyline.

Author Manuscript Author Manuscript Author Manuscript Author Manuscript

sgRNA vector and cloning

The pLKO-based sgRNA vector was purchased Addgene (#52628). The puromycin gene was removed and replaced with a puro-GFP fusion protein previously described [25] using Gibson assembly. The resulting plasmid was digested with BfuAI and incubated with shrimp alkaline phosphatase before isolating the backbone. Complementary sgRNA sequences flanked by ACCG on the 5' end, and CTTT on the 3' of the reverse strand, were annealed, diluted, and ligated into the cut vector with T4 ligase according to the manufacturer's instructions. All transformations were performed in *Stbl3* bacteria and grown at 30° C.

sgRNA Library Construction

The genome-wide Brunello sgRNA library[26] was purchased from Addgene and transformed in *Stbl4* bacteria from Invitrogen. The Brunello library contains 77,441 sgRNAs targeting four unique positions in most (19,114) protein-coding genes, along with 1000 negative control sgRNAs. Sequences for the follow up library of 12,472 sgRNAs were chosen from published sgRNA libraries [27,28] or were designed using the online tool at http://crispr.mit.edu. The library (CustomArray Inc.) of 74-mer of the sgRNA sequence prepended with the oligo sequence GGAAAGGACGAAACACCG and followed by GTTTTAGAGCTAGAAATAGCAAGTTAAAATAAGGC. The oligo library was PCR amplified with Herculase II Fusion DNA polymerase (Agilent) using ArrayF and ArrayR [27]. The subsequent PCR product was gel extracted using an eGel from Invitrogen and 20ng of library was Gibson cloned into BfuAI-cut sgRNA vector following the manufacturer's instructions. Transformations were grown at 30°C overnight on 24.5cm^2 bioassay plates maintaining at least 100X coverage. Colonies were scrapped, spun and DNA was isolated with Blood and Cell Culture DNA Maxi kits (Qiagen).

Virus production and transduction

Lentiviruses were produced in 293FT cells by transfecting sgRNA vectors with packaging vectors pPAX2 (Addgene #12260) and pMD2.g (Addgene #12259) in a 4:3:1 ratio in serum-free Opti-MEM. Trans-IT 293T (Mirus) was added and incubated for 15 minutes before adding dropwise to cells. Supernatants were harvested 24, 48, and 72 hours later, spun at 1000g to pellet any virus producing cells and then incubated with Lenti-X concentrator (CloneTech). Virus was concentrated according to manufacturer's instructions, aliquoted and frozen. Virus titration was performed on target cell populations and GFP was measured 3–4 days later. When GFP was not present in the backbone of the sgRNA plasmids, transduced cells were split and incubated with or without puromycin until untransduced control cells were dead. The percentage of viable cells was then measured by FACS and percent transduction was calculated as the ratio of viable cells in treated versus untreated wells.

Pooled sgRNA screening

For both genome-wide and targeted follow-up screens, individual replicates were transduced such that an average of 500 copies of each sgRNA were present after selection. Cultures were carried for the duration of the 21-day screen maintaining 500X coverage. Antibiotic selection was started 3–4 days after transduction and carried out until untransduced control cells were dead, approximately 4–5 days later. Cells were then harvested for a day 0 time

Author Manuscript Author Manuscript Author Manuscript Author Manuscript

point and doxycycline was added to the culture media at 200ng/mL final concentration. Transduced cells were counted and passaged every two days with fresh media containing dox until day 21 when cells were again harvested for DNA extraction. DNA was isolated from frozen cell pellets using Qiagen QIAmp DNA Blood Midi and Maxi kits.

Library amplification, sequence extraction and PCR primers

For both screens, sgRNA sequences were amplified using a nested PCR to first isolate the sgRNA sequence from genomic DNA and then to add nextgen sequencing adapters compatible with Illumina's NextSeq500. Products were amplified using ExTaq (Takara) for 18 cycles in both rounds of amplification. Products were size selected using an eGel (Invitrogen) and libraries were quantitated using an Illumina specific Kapa quantification kit according to the manufacturer's instructions or by Qubit (Thermo Fisher Scientific). All libraries were sequenced using a high output single-read 75 cycle read flow cell. An average of 400X (200–700X) sequencing depth was achieved. Libraries were multiplexed using indexes compatible with the Illumina TruSeq HT kit with the primers below where x denotes an eight basepair index and y represents a variable length adapter inserted to prevent monotemplate. Eight forward primers and 12 reverse primers were used following this format such that 96 samples could be multiplexed. Basespace.com was used to evaluate sequencing quality measures and to demultiplex sequencing reads. Sequences were aligned to the sgRNAs library allowing for a one basepair mismatch using custom scripts and Bowtie 2 version 2.2.9 with the following parameters: -p 16 -f --local -k 10 --very-sensitive-local -L 9 -N 1.

CRISPR Screen primers

First PCR forward primer:
AATGGACTATCATATGCTTACCGTAACTTGAAAGTATTTCG

First PCR reverse primer: GTAATTCTTTAGTTTGTATGTCTGTTGCTATTATG

Second PCR forward primer:
AATGATACGGCGACCACCGAGATCTACAC**x**ACACTCTTTCCCTACACGACGCTCTTCCGATCT**y**TCTTGTGGAAAGGACGAAACACCG

Second PCR reverse primer:
CAAGCAGAAGACGGCATACGAGAT**x**GTGACTGGAGTTCAGACGTGTGCTCTTCCGATCTCTACTATTCTTTCCCCTGCACTGT

PCR amplification for sgRNA library construction:

ARRAY-F:
TAACTTGAAAGTATTTCGATTTCTTGGCTTTATATATCTTGTGGAAAGGACGAAACACCG

ARRAY-R:
ACTTTTTCAAGTTGATAACGGACTAGCCTTATTTTAACTTGCTATTTCTAGCTCTAAAAC

Author Manuscript Author Manuscript Author Manuscript Author Manuscript

Pooled sgRNA screen analysis

CRISPR screen scores (CSS) were calculated using the following formulas:

Notation: i = [1 – 77,441] Index indicating sgRNA

j = [1 – 11] Index indicating cell line

R_j = Number of replicates for cell line j

r = [1 – R_j] Index indicating replicate

d = [0, 21] index indicating time point

X_{irjd} = Indicates the raw sequencing counts for sgRNA i, in replicate r of cell line j at time d

Step 1: Normalize raw counts by total read counts

$$N_{ir\,jd} = 1 + (X_{ir\,jd} * 4 \times 10^7) / \sum_i X_{ir\,jd}$$

Step 2: Eliminate sgRNAs with low counts across all experimental conditions by calculating

$$m_i = \max_{jd}\left(\min_r N_{ir\,jd}\right)$$

and eliminating those sgRNAs for which $m_i < 100$.

Step 3: Calculate log ratios

$$LR_{ir\,j} = \log_2\left(N_{ir\,j21} / N_{ir\,j0}\right)$$

Step 4: Z transform log-ratios

$$Z_{ir\,j} = \left(LR_{ir\,j} - \operatorname{Mean}_i(LR_{ir\,j})\right) / \operatorname{Standard\ deviation}_i(LR_{ir\,j})$$

Step 5: Average across replicates

$$S_{ij} = \operatorname{Mean}_r(Z_{i\,jr})$$

Step 5: Calculate signal variance for each sgRNA

$$\text{Total Variance: } TV_i = \operatorname{Var}_j(S_{ij})$$

Author Manuscript Author Manuscript Author Manuscript Author Manuscript

$$\text{Error Variance: } EV_i = \underset{j}{\text{Mean}}\left(\underset{r}{\text{Var}}(Z_{ir\,j})/R_i\right)$$

$$\text{Single Variance: } SV_i = TV_i - EV_i$$

Step 6: For each gene g, let G_g be the set of sgRNAs that represent it, and calculate the maximal pair wise correlation between any two sgRNAs in this set.

$$C_g = \underset{k,\,l \in G_g}{\text{Max}}\left(\underset{j}{\text{Correlation}}(S_{kj}, S_{lj})\right)$$

If for a given gene $C_g < 0.45$ then let i_g be the index of the sgRNA representing that gen that has the highest signal variance and use that as the sole representative of gene j

$$Score_{gj} = S_{i_g j}$$

If $C_g \geq 0.45$, then proceed to steps 7 and 8.

Step 7: Average the two sgRNAs which were most correlated within gene *g.*

$$M_{gj} = \frac{1}{2}(S_{kj} + S_{lj})$$

Where $k,l \in G_g$ are such that

$$\text{Correlation}_j(S_{kj}, S_{lj}) = C_g$$

Step 8: For each $i \in G_g$ calculate

$$V_i = \underset{j}{Correlation}\left(S_{ij}, M_{gj}\right)/C_g$$

Average together those sgRNAs for which $V_i > 0.85$ to arrive at final CSS for gene g

$$CSS_{gj} = \underset{i \in G_g,\, V_i > 0.85}{\text{mean}}(S_{ij})$$

For the replication sgRNA library, in which most genes had 9–10 sgRNAs per gene, we found this could be simplified by using the z-scores of the averaged $\log_2$ fold change of all sgRNAs per gene. As described above, using the best correlated sgRNAs per gene excluded many poor performing sgRNAs, it also excluded many high performing sgRNAs that shared expected subtype-specific toxicities.

Author Manuscript Author Manuscript Author Manuscript Author Manuscript

Statistical significance

The statistical significance in Figure 1 of the CSS of ABC BCR-dependent, or GCB DLBCL, compared to all other cell lines, was calculated with a two sided Random Variance T-test [29] for individual genes. Screen correlations were calculated using a Pearson correlation on gene-level metrics in GraphPad Prism 7.0 software on genes displayed in Extended data Fig. 2.

FACS analysis

Cell lines were transduced with sgRNA vectors marked by GFP. Three to four days after transduction, GFP levels were measured by flow cytometry on a BD FACS Calibur using CellQuest™ Pro version 6.0 and analyzed with FlowJo version 9. Cells were split every other day into doxycycline containing media and GFP levels were followed for 14 days and normalized to the day 0 measurement. All sgRNA and shRNA sequences are listed below. When surface proteins were targeted, knockout was validated by flow cytometry by spinning cells down, washing in FACS buffer (PBS plus 2% (vol/vol) FBS, 1mM EDTA), and stained at 4°C for 30 minutes in FACS buffer with fluorescently labeled antibodies: mouse anti-human CD19-APC (Biolegend SJ25C1, 1:500), mouse anti-human CD81-PE (Biolegend 5A6, 1:500), mouse anti-human IgM-APC (MHM-88), 1:400); or from Southern Biotech: goat anti-human IgG-PE (1:200).

Drug sensitivity assays

DLBCL cell lines were enumerated and 10,000 cells were seeded in triplicate in a 96-well plate in fresh media. Ibrutinib (Selleck Chem) was dissolved in DMSO and equal volumes of diluted drug were added to cells to reach the indicated final concentration. Cells were cultured with drugs, which were replenished after 48 hours. Metabolic activity was measured at day 4 by adding 10 ul of MTS reagent (Promega) and incubating at 37°C for 4 hours. Absorbance was measured at 490 nm using a 96-well Tecan Infinite 200 Pro plate reader. Absorbance from media-only wells were subtracted and data was normalized to DMSO control unless otherwise stated. GR50 was calculated using the online tool GRcalculator (http://www.grcalculator.org/) [30]. Drug matrix screens and Δbliss calculations were performed as previously described[31].

Gene Expression Profiling and Signature Enrichment

Cells were transduced with shRNAs, puro-selected and harvested at indicated times after shRNA induction. RNA was isolated using RNEasy mini kits (Qiagen). Gene expression was assessed using two-color human Agilent 4 × 44K gene expression arrays following the manufacturers protocol. Briefly, control shSC4 (control, Cy3-labelled) RNA was compared to RNA from cells with shRNAs targeting TLR9 (C4), TLR9 (D7), MyD88 (A7), MyD88 (B3) (Cy5-labelled) at each of the indicated time points. Array elements were filtered for spot quality using Agilent Feature Extraction software version 10.7, specific genes were determined to be downregulated if the $\log_2$ fold change (comparing control shSC4 to shRNA for TLR9) was less than −0.3 for at least 3 of the 4 time points (shTLR9) per cell line. Gene expression data have been deposited in Gene Expression Omnibus (GEO) under accession GSE99276. Signature enrichment was performed as previously described [32]. Briefly,

Author Manuscript Author Manuscript Author Manuscript Author Manuscript

downregulated genes were tested for overlap with published gene signatures in a 2×2 contingency table using a Fisher's exact test.

DNA Copy Number analysis

DLBCL DNA samples were analyzed with the Affymetrix SNP6.0 array. Probe log ratios were calculated using Affymetrix Genotyping Console, and were collected into segments of similar value using circular binary segmentation (http://www.bioconductor.org/packages/3.7/bioc/manuals/DNAcopy/man/DNAcopy.pdf). These segments were assigned copy number values as previously described [33] without segment length restrictions. DNA copy number was correlated to sample gene expression using linear regressions calculated with Graphpad Prism version 7.0. Amplified regions were identified and visualized on the UCSC genome browser, Hg19.

NF-κB reporters

The generation of the IκBα luciferase reporter cell line has been previously described [34]. Briefly, TMD8-IκBα cell line was transduced with indicated shRNAs, puro-selected and induced with doxycycline. Cells were harvested at the indicated time points and luciferase was measured with the Dual Luciferase Reporter Assay System (Promega) on a Tecan Infinite 200 Pro plate reader.

IgM co-immunoprecipitation

HBL1, TMD8, OCI-Ly10 and OCI-Ly19 cells were lysed at 10^7 cells per ml in a modified RIPA buffer (0.5% Triton X-100, 0.25% deoxycholate, 0.025% SDS, 10 mM Tris, pH 8.0, 100 mM NaCl, 10 mM EDTA, 1 mM Na_3VO_4, 30 mM pyrophosphate, 10 mM glycerophosphate, 1 mM AEBSF, 0.02 U ml^{-1} aprotinin and 0.01% NaN_3) for 10 min. on ice. Lysates were cleared by centrifugation at 14,000xg for 20 min. at 4°C. IgM was immunoprecipitated by incubating lysates on ice for 1 hour with 10 μg of biotin-labeled goat anti-human IgM (Jackson Immunoresearch), followed by the addition of 35 μl of pre-washed streptavidin-agarose beads (Invitrogen) and rotated for 30 min. at 4°C. Beads were washed 3X with cold 1X RIPA buffer, then solubilized by adding 2X LDS sample buffer (Invitrogen) with 1% β-mercaptoethanol and boiled for 5 min. Samples were separated on a 10% polyacrylamide gel and transferred to Immobilon-p PVDF membrane (Millipore) for western blot analysis. Membranes were probed with rabbit anti-TLR9 monoclonal XP, rabbit anti-TLR7 (Cell Signaling Technologies), rabbit anti-TLR4 (Santa Cruz Biotechnology) and goat anti-IgM-HRP (Bethyl).

Proximity Ligation Assay

DLBCL cell lines were either left untreated, treated with 10 nM ibrutinib, 200 nM AZD2014 or equivalent volumes of DMSO, or transduced with either control shRNA (SC4) or shRNAs targeting CD79A, TLR9, MYD88, CARD11, BCL10 or MALT1, followed by puromycin (Invitrogen) selection as previously described [35]. Cells were plated onto a 15 well μ-Slide Angiogenesis ibiTreat chamber slide (Ibidi) and allowed to adhere to the surface for 30 min at 37°C. Cells were then fixed with 4% paraformaldehyde (Electron Microscopy Sciences) for 20 min at room temperature and then washed in PBS (Invitrogen). Cellular membranes

Author Manuscript Author Manuscript Author Manuscript Author Manuscript

were labeled with 5 μg/ml wheat germ agglutinin (WGA) conjugated to Alexa Fluor 488 (Thermo Fisher Scientific) for 10 min at room temperature. Cells were permeabilized in cold methanol for 10 min, washed in PBS and then blocked in Duolink Blocking buffer (Sigma) for 30 min at room temperature. Primary antibodies were diluted in Duolink Antibody Diluent (Sigma) and incubated overnight at 4°C (See Supplemental Table S8). Where appropriate, cells were counterstained with mouse anti-Lamp1 conjugated to Alexa Fluor 405 (Santa Cruz Biotechnology) with the primary antibodies. The following morning, cells were washed for 20 min in a large volume of PBS with 1% BSA, followed by addition of the appropriate Duolink secondary antibodies (Sigma), diluted and mixed according to the manufacturer's instructions. Cells were incubated for 1 hour at 37°C, after which cells were washed in TBST with 0.5% tween-20 for 10 min. Ligation and amplification steps of the PLA were performed using the Duolink in situ Detection Reagents Orange kit (Sigma) according to the manufacturer's instructions. Following the PLA, cells were mounted in Prolong Gold mounting media with DAPI (Invitrogen). Images were acquired on a Zeiss LSM 880 Confocal microscope using Zeiss Zen Black version 2.3. Images for display and Pearson's correlation coefficients values were calculated with NIH ImageJ/FIJI software version 2.0.0-rc-65/1.5ls [36]. PLA spots were counted in cell lines using Blobfinder version 3.2 [37]. PLA Score was determined by normalizing the number of PLA spots counted in each sample to the average number of PLA spots counted in the control sample, which was set to 100. Box and whisker plots display the median PLA Score with whiskers incorporating 10–90% of all data, outliers are displayed as dots.

The PLA was performed on formalin-fixed, paraffin-embedded (FFPE) tissue microarrays or biopsy samples in a similar manner. FFPE microarrays (7 μm) and patient tissue sections (4 μm) were deparaffinized in xylene and rehydrated in graded alcohol and distilled water. Heat induced antigen retrieval was performed on TMAs and tissue sections at pH 6.0 for 30 minutes. Slides were then placed in tris-buffered solution and prepared for proximity ligation assay, as described above, samples were costained with mouse anti-human CD20-eFluor660 or AlexaFluor488 (L26, eBioscience). Data was analyzed using Blobfinder version 3.2. Cells with 10 or more IgM:TLR9 puncta in their nucleus were removed from analysis to control for increased autofluorescence in FFPE samples. Tissue microarrays were prepared by fixing cells in neutral buffer formalin for 24 hours, pelleting, and resuspending in an equal volume of low-melt agarose in a 10 ml conical tube. The resulting pellet was paraffin embedded by standard protocol [38]. The resultant blocks were used to construct a cell line array (CMA) using the same approach used for construction of a tissue microarray, with 1.00 mm needles, using a Beecher MTA-1 instrument (Beecher Instruments, Silver Spring, MD). Sample identifiers were removed and blinded before pathology review for PLA signal. After all data was collected, sample identifiers were revealed and samples were grouped by response to ibrutinib.

BioID2 contructs

BioID2 (Addgene #80899) was appended to the c-terminus of TLR9 and MYD88^{L265P} using Gibson cloning techniques. MYD88^{L265P}-13X-BioID2 was cloned by removing GFP from the previously described pBMN-MYD88^{L265P}-VD-GFP [35] by restriction digest with

Author Manuscript Author Manuscript Author Manuscript Author Manuscript

StuI and NotI. BioID2 was PCR amplified with a 13X N-terminal linker and Gibson cloned as above from Addgene #80899 with the following primers:

MYD88-Cterm/13X: CTGGACTCGCCTTGCCAAGGCCTTGTCCCTGCCCGGTGGAGGCGGGTCTGGAGGC

pBMN-NotI-BioID2-Cterm: CCTCTAGTGCGGCCGCTTATGCGTAATCCGGTACATC

BioID2 was also appended to the c-terminus of both wild type and mutant isoforms of MYD88 with a two-amino acid linker (VD). First, BioID2 and MYD88 were PCR amplified with Primestar (Takara) using the following primers:

BioID FWD: TTGTCCCTGCCCGTCGACTTCAAGAACCTGATCTGGCTG

BioID REV: CGCCGGCCCTCGAGGCTATGCGTAATCCGGTACATCG.

MYD88 FWD:AATTCGAATTCCTGAAGGGCCACCATGCGACCCGACCGCGC

MYD88 REV: AGATCAGGTTCTTGAAGTCGACGGGCAGGGACAAGGC

TLR9 was cloned into a modified version of pBMN that expresses a 10X linker followed by BioID2 with the following oligos.

TLR9 C-BioID FWD: CTGCCGGATCCGAATTCTA GCC ACA atgggtttctgccgcagcg

TLR9 C-BioID REV: CCCGACCCGCCTCCACCTAC ttcggccgtgggtccctggc

The PCR products were separated on a 1% agarose gel and column purified (Qiagen). Purified PCR products were mixed and added to pBMN-LYT2 vector that was linearized with StuI (New England Biolabs) and subjected to a Gibson reaction (New England Biolabs) following the manufacturer's protocol.

Imaging MYD88–13X-BioID2

$MYD88^{L265P}$-13X-BioID2 was retrovirally transduced into TMD8 cells, and then purified with anti-LYT2 beads as described above. Cells were first cultured for 16 hr in 50μM biotin. Next, cells were incubated with 1μg/ml goat anti-human IgM FAB conjugated to Alexa Fluor 488 (Jackson Immunoresearch) for 90 min at 37°C. During this incubation period, cells were plated onto a 15 μ-Slide 8 well IbiTreat chamber slides (Ibidi) for 30 min and allowed to stick to the slides. Cells were washed 2X with PBS and then fixed with 4% paraformaldehyde (Electron Microscope Sciences) for 20 min and then permeabilized with cold methanol for 10 min at −20°C. Fixed and permeabilized cells were blocked with Duolink blocking buffer (Sigma) for 30 min at room temperature. Cells were then incubated with rabbit mAb anti-phospho-IKKα/β (Ser176/180) (Cell Signaling Technology) diluted 1:200 in PBS with 1% BSA for 2 hour at room temperature, followed by 2X washes with PBS:BSA. Cells were then incubated with anti-rabbit F(ab')2 conjugated to Alexa Fluor 555 (Cell Signaling Technology) at 1:1000, mouse anti-Lamp1 conjugated to Alexa Fluor 405 (Santa Cruz Biotechnology) at 1:50 and streptavidin conjugated to Alexa Fluor 647

Author Manuscript Author Manuscript Author Manuscript Author Manuscript

(Biolegend) at 1:1000, all diluted into PBS:BSA and allowed to incubate for 1 hour at room temperature. Cells were then washed for 15 min in a large volume of PBS:BSA and mounted with Prolong Diamond mounting media (Invitrogen). Images were acquired on a Zeiss LSM 880 Confocal microscope. Images for display were prepared with NIH ImageJ/FIJI [36] and animations were prepared using the Imaris 3D rendering software (Bitplane). The number of BioID2 puncta and their intensity were quantified from z-stack images (1 μm slices) using Blobfinder.

In certain instances, TMD8, OCI-Ly10 and/or HBL1 cells expressing $MYD88^{L265P}$-13X-BioID2 were additionally transduced with either control shRNA (SC4) or shRNAs targeting CD79A, TLR9 or MYD88, as described above. Following puromycin (Invitrogen) selection, cells stained with streptavidin conjugated to Alexa Fluor 555 (Thermo Fisher Scientific) and anti-LYT2 conjugated to Alexa Fluor 647 (Biolegend). Cells were either subjected to FACS analysis, as described above, or were imaged as described above. Biotin spots or blobs were counted using Blobfinder, as for the PLA above. Likewise, these cell lines were either left untreated, treated with 10nM ibrutinib or equivalent volumes of DMSO, then stained and analyzed in the same manner.

Mass spectrometry and western blot analysis of BioID2 constructs

TLR9–10X-BioID2 pBMN-LYT2 and MYD88–13X-BioID2 pBMN-LYT2 constructs were retrovirally transduced into DLBCL cell lines, as described above. Infected cells were enriched by positive selection with LYT2 magnetic beads (Invitrogen). Cells were then grown in SILAC media, containing amino acids labeled with stable isotopes or arginine and lysine, for 2 weeks prior to expansion to 100×10^6 cells. In certain cases, cells were treated with either 10 nM ibrutinib or 200 nM AZD2014 for 24 hours. 16 hours prior to lysis, biotin (Sigma) was added to a final concentration of 50μM to transduced cells. Cells were then lysed at 2.5×10^7 cells per ml in RIPA buffer modified for MS analysis (1% NP-40, 0.5% deoxycholate, 50 mM Tris, pH 7.5, 150 mM NaCl, 1 mM Na_3VO_4, 5mM NaF, 1 mM AEBSF) for 10 min. on ice. Lysates were cleared by centrifugation at 14,000xg for 20 min. at 4°C. 35μl of Pre-washed streptavidin agarose beads were added to each sample; samples were then rotated at 4°C for 2 hours, then washed four times in 1X RIPA buffer, then solubilized with 4X LDS sample buffer (Invitrogen) with 1% β-mercaptoethanol, and boiled for 5 min. A fraction of lysates were also subjected to western blot analysis as described above. Western blots were probed with rabbit anti-CARD11 and rabbit anti-MALT1 (Cell Signaling Technologies) and mouse anti-MYD88 (Santa Cruz Biotechnology).

For MS analysis, proteins were separated by one-dimensional gel electrophoresis (4–12% NuPAGE Bis-Tris Gel, Invitrogen, USA) and the entire lane of a Coomassie blue-stained gel was cut into 23 slices. All slices were processed as described previously [39] After tryptic digestion of the proteins the resulting peptides were resuspended in sample loading buffer (2% acetonitrile and 0.05% trifluoroacetic acid) and were separated by an UltiMate 3000 RSLCnano HPLC system (Thermo Fisher Scientific) coupled online to a Q Exactive HF mass spectrometer (Thermo Fisher Scientific). First, peptides were desalted on a reverse phase C18 precolumn (Dionex 5 mm length, 0.3 mm inner diameter) for 3 minutes. After 3 minutes the precolumn was switched online to the analytical column (30cm length, 75 mm

Author Manuscript Author Manuscript Author Manuscript Author Manuscript

inner diameter) prepared in-house using ReproSil-Pur C18 AQ 1.9 mm reversed phase resin (Dr. Maisch GmbH). Buffer A consisted of 0.1 % formic acid in H_2O, and buffer B consisted of 80% acetonitrile and 0.1% formic acid in H_2O. The peptides eluted from buffer B (5 to 42 % gradient) at a flow rate of 300 nl/min over 76 min. The temperature of the precolumn and the analytical column was set to 50°C during the chromatography. The mass spectrometer was operated in a TopN data-dependent mode, where the 30 most intense precursors from survey MS1 scans were selected with an isolation window of 1.6 Th for MS2 fragmentation under a normalized collision energy of 28. Only precursor ions with a charge state between 2 and 5 were selected. MS1 scans were acquired with a mass range from 350 to 1600 m/z at a resolution of 60,000 at 200 m/z. MS2 scans were acquired with a starting mass of 110 Th at a resolution of 15,000 at 200 m/z with maximum IT of 54ms. AGC targets for MS1 and MS2 scans were set to 1E6 and 1E5, respectively. Dynamic exclusion was set to 20 seconds.

MS data analysis

MS data analysis was performed using the software MaxQuant (version 1.6.0.1) linked to the UniProtKB/Swiss-Prot human database containing 155990 protein entries and supplemented with 245 frequently observed contaminants via the Andromeda search engine.[40] Precursor and fragment ion mass tolerances were set to 6 and 20 ppm after initial recalibration, respectively. Protein biotinylation, N-terminal acetylation and methionine oxidation were allowed as variable modifications. Cysteine carbamidomethylation was defined as a fixed modification. Minimal peptide length was set to 7 amino acids, with a maximum of two missed cleavages. The false discovery rate (FDR) was set to 1% on both the peptide and the protein level using a forward-and-reverse concatenated decoy database approach. For SILAC quantification, multiplicity was set to two or three for double (Lys +0/Arg+0, Lys+8/Arg+10) or triple (Lys+0/Arg+0, Lys+4/Arg+6, Lys+8/Arg+10) labeling, respectively. At least two ratio counts were required for peptide quantification. The "re-quantify" option of MaxQuant was enabled. Data was filtered for low confidence peptides.

Xenograft

All mouse experiments were approved by the National Cancer Institute Animal Care and Use Committee (NCI-ACUC) and were performed in accordance with NCI-ACUC guidelines and under approved protocols. Approved protocols allowed tumor growth below 20mm in any dimension; no animals had tumors which exceeded these limits. Female NSG (non-obese diabetic/severe combined immunodeficient/common gamma chain deficient) mice were obtained from NCI Fredrick Biological Testing Branch and used for the xenograft experiments between 6–8 weeks of age. TMD8 tumors were established by subcutaneous injection of 10×10^6 cells in a 1:1 Matrigel/PBS suspension. Treatments were initiated when tumor volume reached a mean of $200mm^3$. Ibrutinib was prepared in PBS with 50% (v/v) DMSO and administered i.p. once per day (5mg/kg/day). AZD2014 was prepared in deionized water with 1% (v/v) Tween 80 and administered p.o. once per day (15mg/kg/day). For ADZ2014/ibrutinib combination, drugs were given at the same concentration and schedule as single agents. Tumor growth was monitored every other day by measuring tumor size in two orthogonal dimensions and tumor volume was calculated by the following

Author Manuscript Author Manuscript Author Manuscript Author Manuscript

equation: tumor volume = (length × width^2)/2. reatment randomization and experimenter blinding were not possible. Sample size was estimated based upon preliminary experiments.

FFPE Biopsies

All cases were either needle aspirates, whole lymph node biopsies, or were obtained from surgically removed specimens. Samples were fixed in 10% buffered formalin for 18–24 hours and paraffin embedded for long term storage. Samples were studied in accordance with the ethics and principles of the Declaration of Helsinki and under Institutional Review Board approved protocols from the National Cancer Institute National Institutes of Health Protocol Review Office (protocol numbers 10-C-0181, 10-CN-074 C, 00-C-133, 00-C-133) or Johns Hopkins School of Medicine (IRB00154052). Informed consent was obtained from all patients or given an IRB-waiver as archived tissue submitted for consultation to the Hematopathology Section. All samples were anonymized or de-identified for subsequent PLA analysis.

shRNA and sgRNA sequences used in functional assays

shSC4 (MSMO1 ex5) CTCTCAACCCTTTAAATCTGA,

shCD19 (3’ UTR) GATTCACACCTGACTCTGAAA,

shCD79A (3’ UTR) GGGGCTTCCTTAGTCATATTC,

shTLR9 #1 (N133) GAGCTAAACCTGAGCTACAAC

shTLR9 #2 (3’ UTR) GCACGGTGCCACCTCCACACT,

shMYD88 #1 (3’ UTR) GTACCAGTATTTATACCTCTA

shMYD88 #2 (ex3) GGCATATGCCTGAGCGTTTC,

shBCL10 #2 (3’ UTR) CTGACATTGTCTCCTATATA,

shCARD11 (3’ UTR) GGGGTGTGTACCAGGCTATGA,

sgTLR9 #8 GACCAGGCTCCCGAAGGAAG,

sgMYD88 #10 CCGGCAACTGGAGACACAAG,

sgUNC93B1 #B73 TGTTGCCATACTTCACCTCG,

sgCNPY3 #9 TCAGCACGTGGTTGGCGCAG,

Data availability

The datasets generated for these analyses are included in the supplementary materials, or have been deposited under accession numbers GSE99276 (GEO). Primary sequencing data and copy number analysis DLBCL cases will be made available through the NIH dbGAP system (accession numbers phs001444, phs001184 and phs000178, https://

Author Manuscript Author Manuscript Author Manuscript Author Manuscript

www.ncbi.nlm.nih.gov/projects/gap/cgi-bin/study.cgi?study_id=phs001444.v1.p1) and the NCI Genomic Data Commons.

Code availability

All computer code is available at https://lymphochip.nih.gov/local/CRISPR/. Gene expression data have been deposited in Gene Expression Omnibus (GEO) under accession GSE99276. All CRISPR screen data, SILAC-MS, and genomic data used in the manuscript are included in supplementary tables.

Author Manuscript
Author Manuscript
Author Manuscript
Author Manuscript

Extended Data

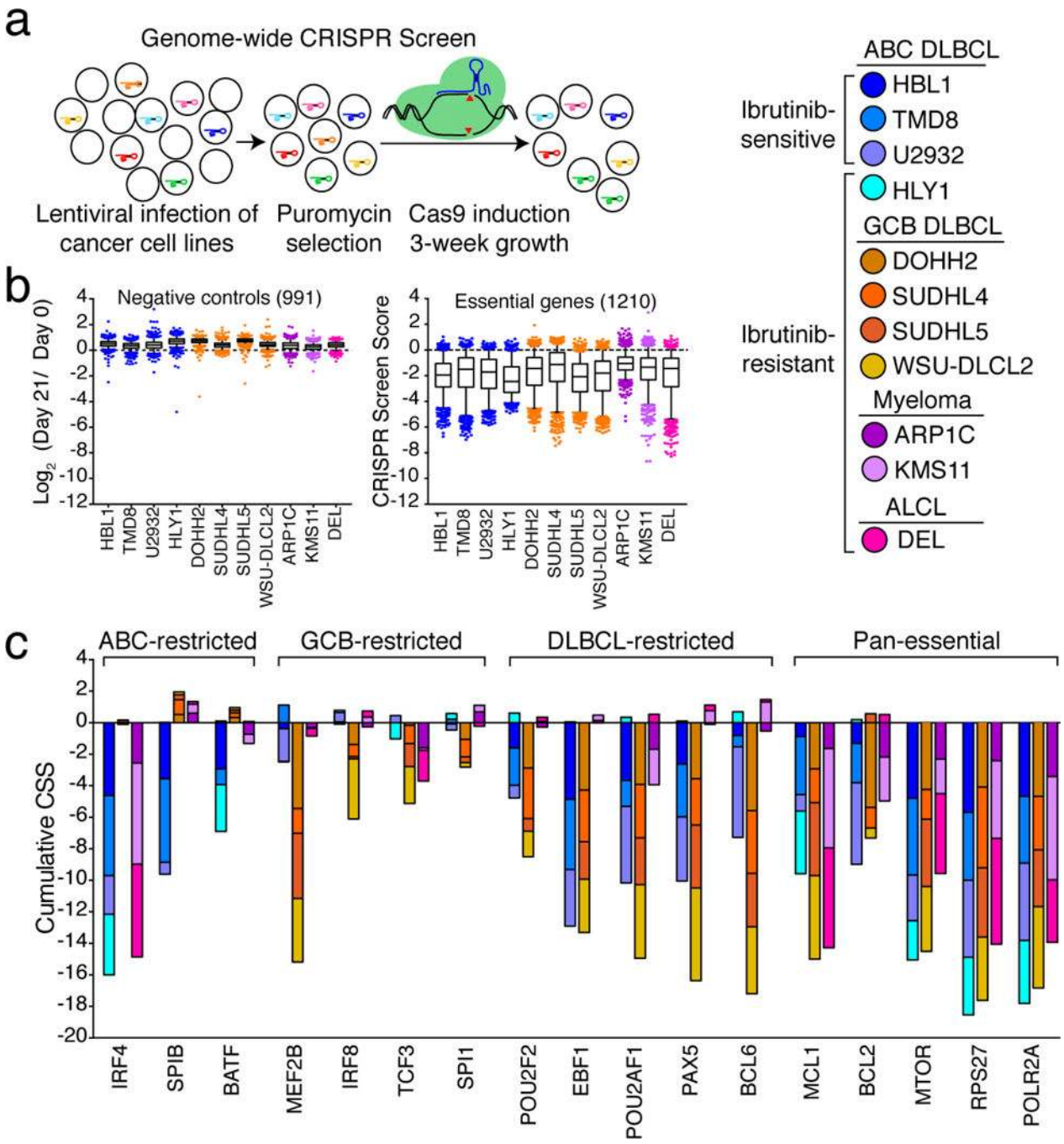

Extended Data Figure 1. CRISPR screen controls.

a, Schematic of CRISPR-Cas9 screens in lymphoma cell lines. **b,** 991 negative control non-targeting (left) or 1210 positive control, essential gene (right) targeting sgRNAs are displayed for each cell line with indicated metrics. Box and whisker plots display mean and interquartile data, outliers represent 10% of total dataset. **c**, Cumulative CRISPR screen scores for indicated genes are displayed for lymphoma cell lines screened.

Author Manuscript Author Manuscript Author Manuscript Author Manuscript

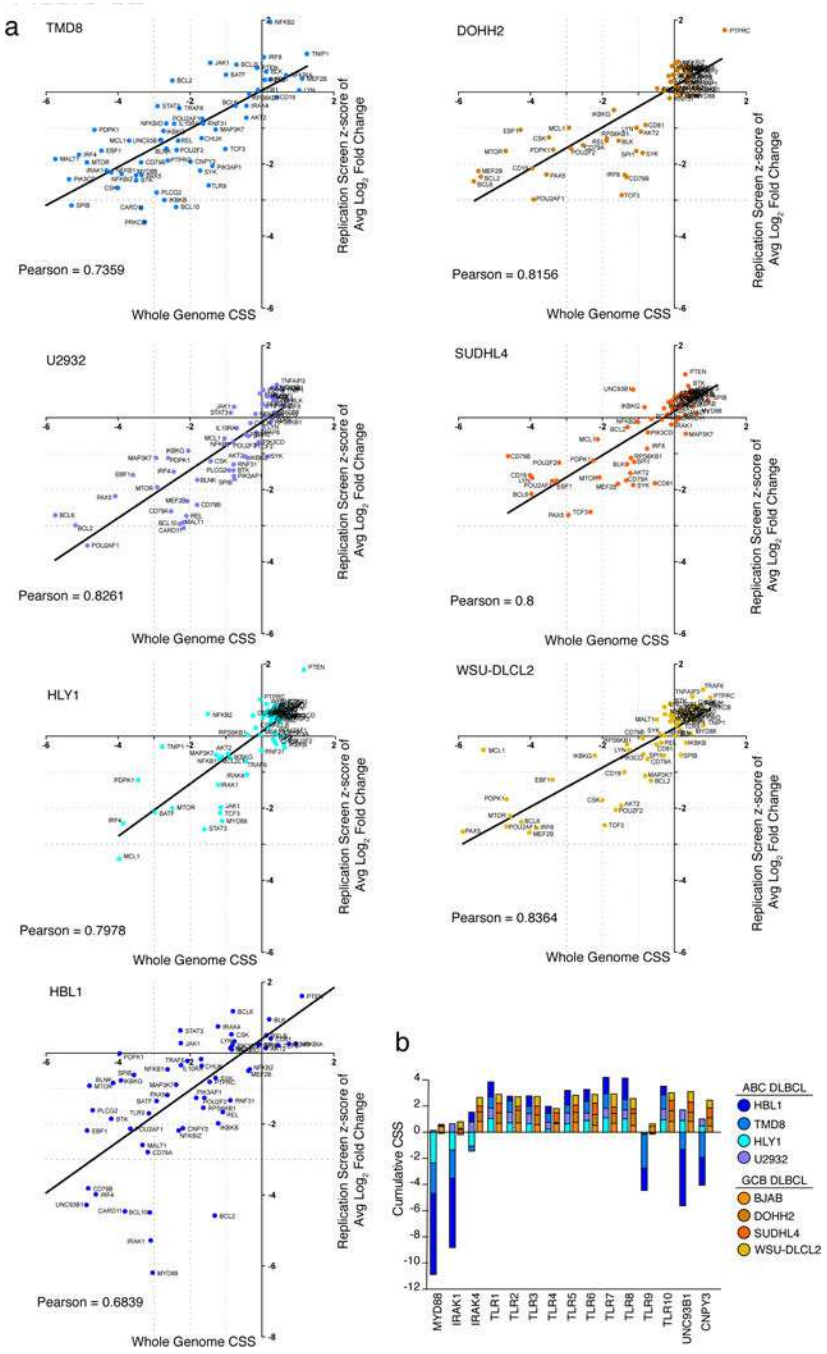

Extended Data Figure 2. Correlation of genome-wide and replication CRISPR screens.

A subset of lymphoma cell lines were rescreened with replication libraries sgRNAs targeting each of the displayed 62 genes. Depletion scores of the genome-wide screen are shown on the x-axis while the z-score of the average $\log_2$ fold change of all sgRNAs targeting a given gene is shown on the y-axis for the replication screen. Pearson correlations (n=62) and linear regressions are displayed for each of the overlapping datasets. **b**, Cumulative CRISPR screen scores for TLR-pathway genes are displayed for ABC (blue) and GCB (orange) DLBCL cell lines.

Author Manuscript Author Manuscript Author Manuscript Author Manuscript

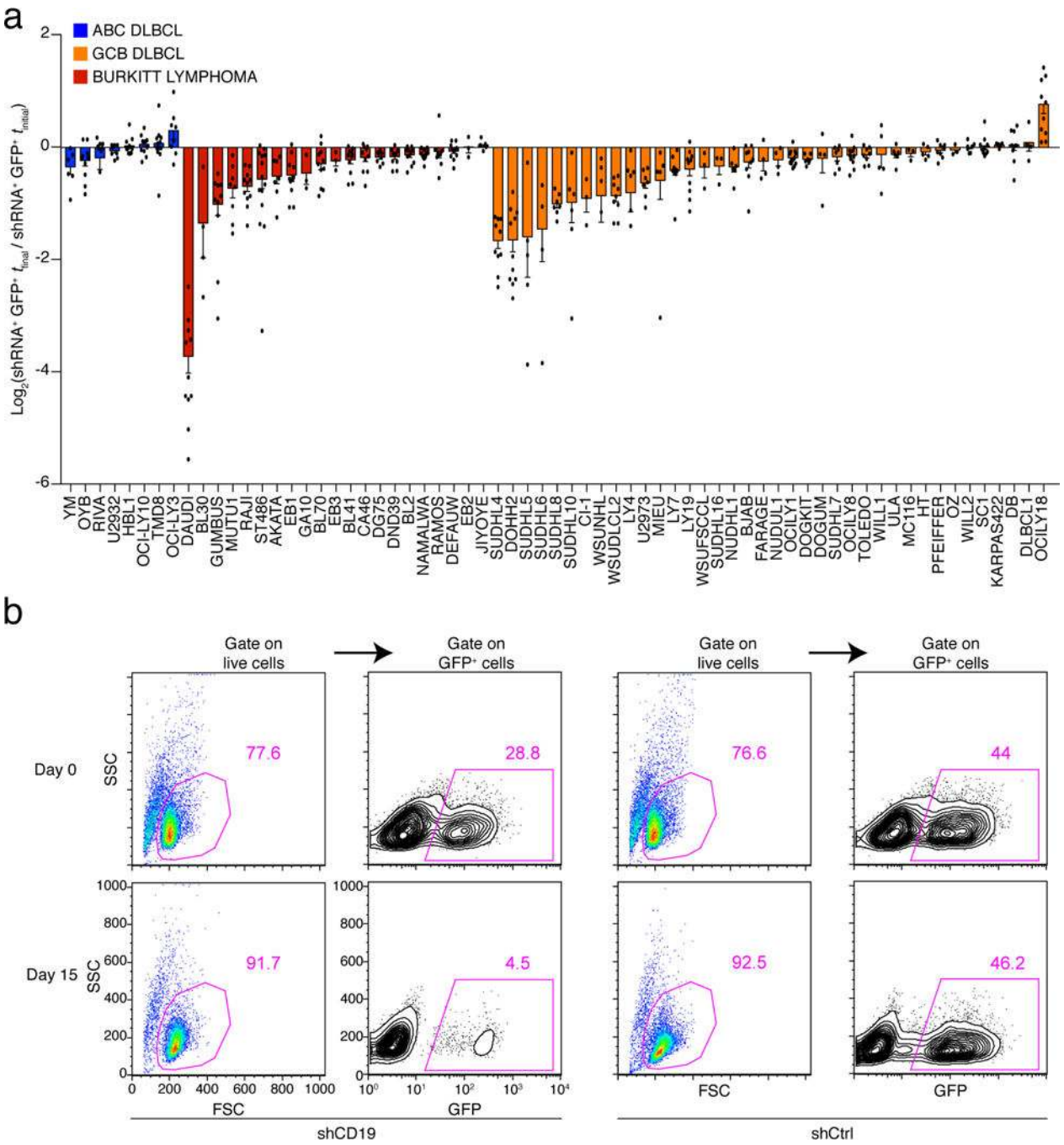

Extended Data Figure 3. CD19 is required for GCB and Burkitt lymphoma survival.

a, A panel of 67 lymphoma cell lines was transduced with an shRNA targeting CD19. Shown is the log ratio of the percent of live, shRNA-containing (GFP+) cells at the last time point (t_{final} ,10–12 days) versus the intial time point ($t_{initial}$, day 0). ABC lines are depicted in blue, GCB lines depicted in orange, and BL lines are depicted in dark red. Average and SEM are displayed from independent biological replicates. See Statistics and Reproducibility. **b**, FACS gating strategy for Live, GFP$^+$ shRNA or sgRNA expressing cells with knockdown of CD19 or negative control genes.

Author Manuscript
Author Manuscript
Author Manuscript
Author Manuscript

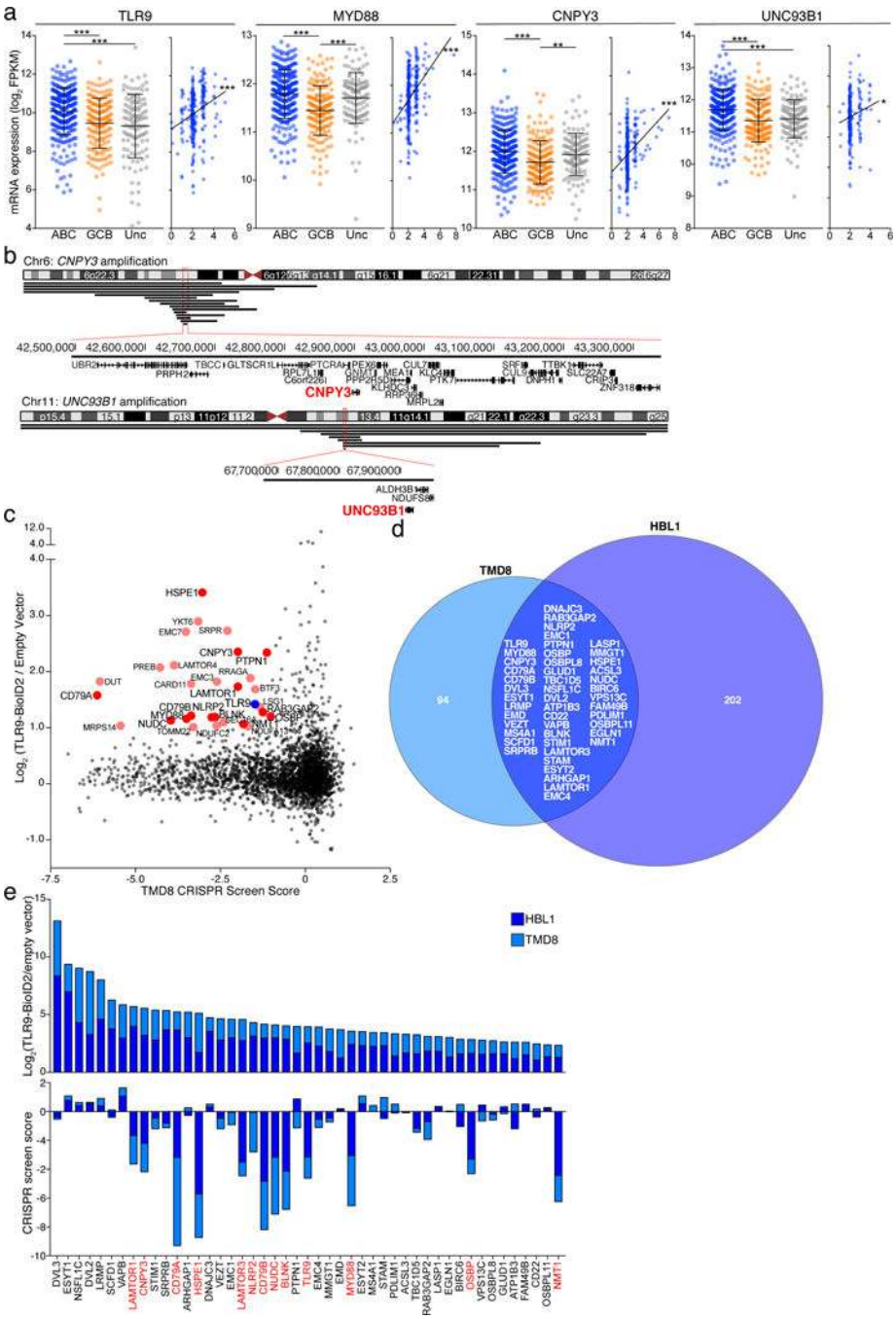

Extended Data Figure 4. TLR9 overexpression and association with the BCR are features of ABC DLBCL.

a, Gene expression values (Log_2 FPKM) values of TLR9 associated genes are shown by DLBCL subtype, ABC in blue (n=294), GCB in orange (n=164) and unclassified (Unc) in grey (n=115). Gene expression data was correlated with DNA copy number and linear regression calculated for ABC samples. One-way ANOVA and Tukey's post test *p< 0.05 ***p< 0.001 (left), linear regression *p< 0.05 ***p<0.0001 (right). **b,** Amplification of the UNC93B1 and CNPY3 loci (black lines, below chromosome ideogram). Minimal shared

Author Manuscript Author Manuscript Author Manuscript Author Manuscript

amplified regions in ABC DLBCL biopsies are bracketed and genes displayed below. **c,** The essential TLR9 interactome in TMD8. TLR9-BioID2 interactome determined by SILAC-based mass spectrometry (y-axis) plotted by the CRISPR screen score (CSS, x-axis). Bait (TLR9) is labeled in blue. Essential interactors are labeled in red, those shared with HBL1 (Fig. 2C) are labeled in dark red. **d,** Venn diagram of the overlap of SILAC mass spectrometry TLR9-BioID2 interactors in experiments performed in TMD8 and HBL1 ABC lines. The 47 overlapping proteins are listed. **e,** The enrichment of 47 overlapping TLR9-bioID2 proximal proteins is shown (upper) relative to their CRISPR screen score (lower). Gene names labeled in red are enriched and toxic to both HBL1 and TMD8. See Statistics and Reproducibility.

Author Manuscript
Author Manuscript
Author Manuscript
Author Manuscript

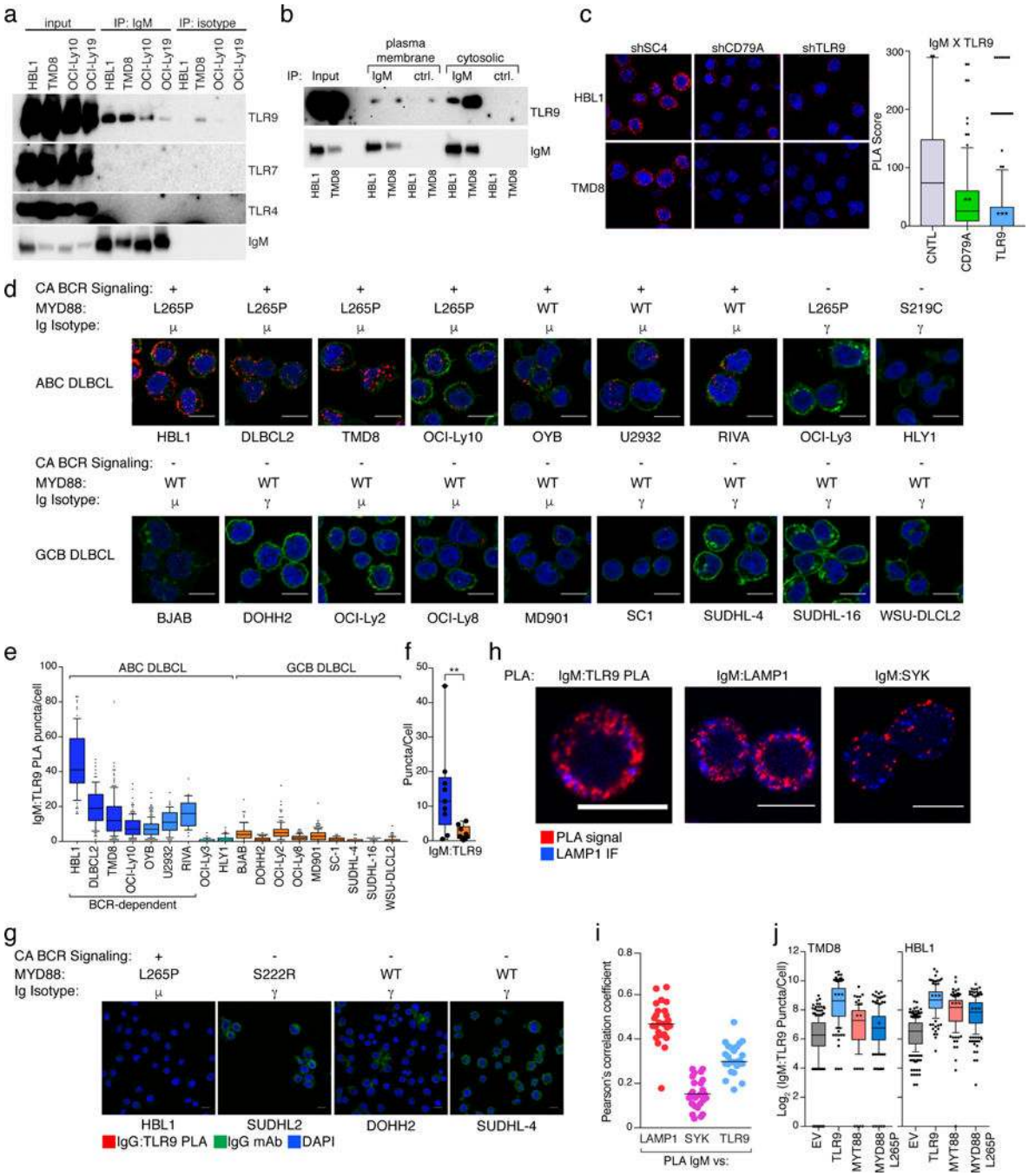

Extended Data Figure 5. IgM interacts with intracellular TLR9 in ABC DLBCL lines.

a, Whole cell lysates of indicated DLBCL cell lines were immunoprecipitated with anti-IgM or isotype control antibodies before being immunoblotted with IgM or indicated TLR antibodies, representative blots, n=3. **b,** ABC DLBCL cell lines HBL1 and TMD8 were incubated on ice with IgM or isotype control antibodies and lysed. Lysates were immunoprecipitated (plasma membrane) with IgM or isotype control. Unbound lysates (cytosolic) were then immunoprecipitated with IgM or isotype control antibodies before all IP lysates were immunoblotted with indicated antibodies, representative blots, n=2. **c,**

Author Manuscript Author Manuscript Author Manuscript Author Manuscript

Confocal images of PLA reaction between IgM and TLR9 in HBL1 and TMD8 cells transduced with control SC4, CD79A or TLR9 shRNAs. Cells were puromycin selected and shRNAs induced with dox for two days before being fixed and imaged (left); quantification right, data from 3 separate experiments. Data are pooled biologically independent experiments of n>100 cells scored per condition. Box plots represents median and 25–75% of data, whiskers display 10–90 percentile; one-way ANOVA with Dunnett's post test, ***p<0.001, **p<0.001. **d,** An IgM:TLR9 PLA (red) was performed in a panel of ABC and GCB DLBCL cell lines and the presence of chronic active BCR signaling (+ = present), MYD88 mutational status and IgH isotype (μ=IgM, γ=IgG) are displayed. Nuclei were stained with DAPI (blue) and membranes visualized by WGA (green). **e,** The number of puncta per cell of IgM:TLR9 PLA is quantitated. Box and whisker plots display mean and interquartile data, whiskers display 10–90 percentile. Data are from 3 fields of cells quantitated from 1 representative experiment of 3 biologically independent replicates. **f,** The data from Fig. 5e segregated by ABC (blue, n=9) and GCB (orange, n=9) lines. Box plots represent median and 25–75% of data, whiskers display range; Mann-Whitney unpaired one-tailed t-test **p< 0.01. **g,** IgG:TLR9 PLA (red) was performed in indicated DLBCL cell lines costained with DAPI (blue) and IgG-AlexaF488 (green). MYD88 mutational status, IgH isotype and presence of chronic active BCR signaling (+=present, −=absent) are displayed. Representative data from 2 independent biological replicates. **h,** To define the cytoplasmic location of the BCR-TLR9 interaction, we counterstained ABC cells for LAMP1, a marker of late endolysosomes, where TLR9 resides, and performed PLA between IgM:TLR9, IgM:LAMP1 and IgM:SYK. The PLA signal is in red, LAMP1 is counterstained in blue. Representative data from 3 independent biological experiments. **i,** To quantify the association between PLA signals and LAMP1 staining, we calculated the Pearson's correlation coefficients across all pixels in each imaged cell (n=25 cells/PLA pair). The highest correlation was between an IgM:LAMP1 PLA and LAMP1 staining (R=0.471), whereas the correlation between an IgM:SYK PLA signal and LAMP1 was much lower (R=0.153). The correlation between the IgM:TLR9 PLA signal and LAMP1 staining was intermediate (R=0.310), indicating that a significant component of the IgM:TLR9 interaction is in $LAMP1^{+}$ vesicles. Quantitated data is from one of three independent biological experiments. **j,** Quantitation of IgM:TLR9 PLA signal following ectopic expression of either empty vector, TLR9, wild type MYD88 or $MYD88^{L265P}$. Data pooled from 3 (HBL1) or 2 (TMD8) biologically independent replicates of n ≥100 cells scored per condition. Box plots represents median and 25–75% of data, whiskers display 10–90 percentile; one-way ANOVA with Dunnett's post test, ***p<0.001, **p<0.01, *p<0.05. See Statistics and Reproducibility.

Author Manuscript Author Manuscript Author Manuscript Author Manuscript

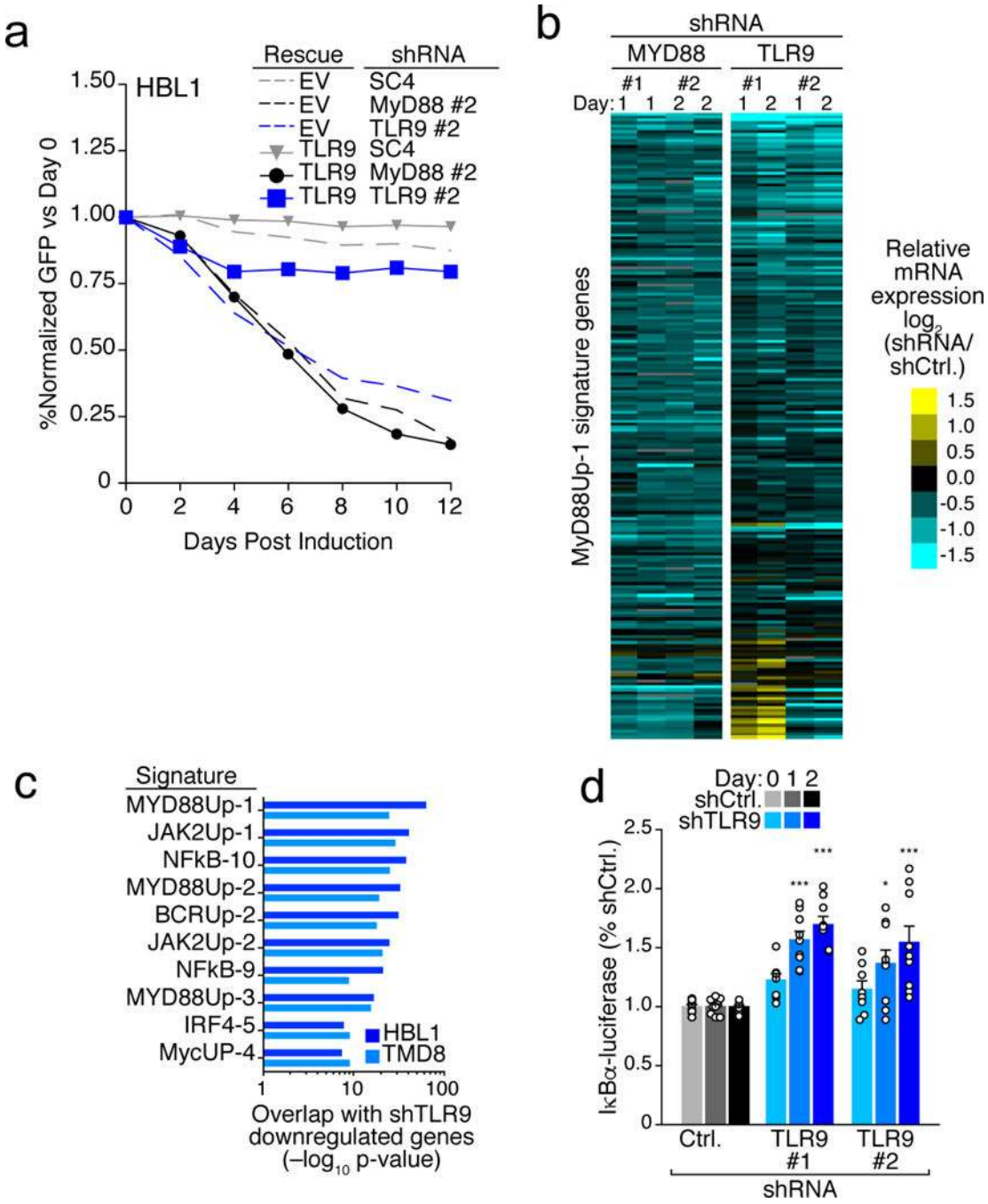

Extended Data Figure 6. TLR9 knockdown phenocopies MYD88 knockdown.

a, TLR9 shRNA is rescued by overexpression of TLR9. HBL1 cells were transduced with empty vector (EV) or wild type TLR9 expressing dsRedExpress2 vectors and then with shRNA vectors marked by GFP targeting a control (SC4), MYD88 or TLR9. The percent of double positive cells was monitored by FACS and normalized to day 0. One of three representative biologically independent experiments is shown. b, Heatmap of gene expression values showing the global phenocopy of MYD88-dependent genes after shRNA-mediated knockdown of TLR9 or MYD88 in HBL1 at indicated time points. c, Gene

signatures enriched in downregulated genes from HBL1 or TMD8 after shRNA-mediated knockdown of TLR9. d, Normalized IκBα—luciferase reporter levels at indicated time points after knockdown of TLR9 with indicated shRNAs; mean and SEM are shown of nine technical replicates from n=3 independent biological experiments. One-way ANOVA with Sidak's multiple comparison test, *p<0.05, ***p<0.001.

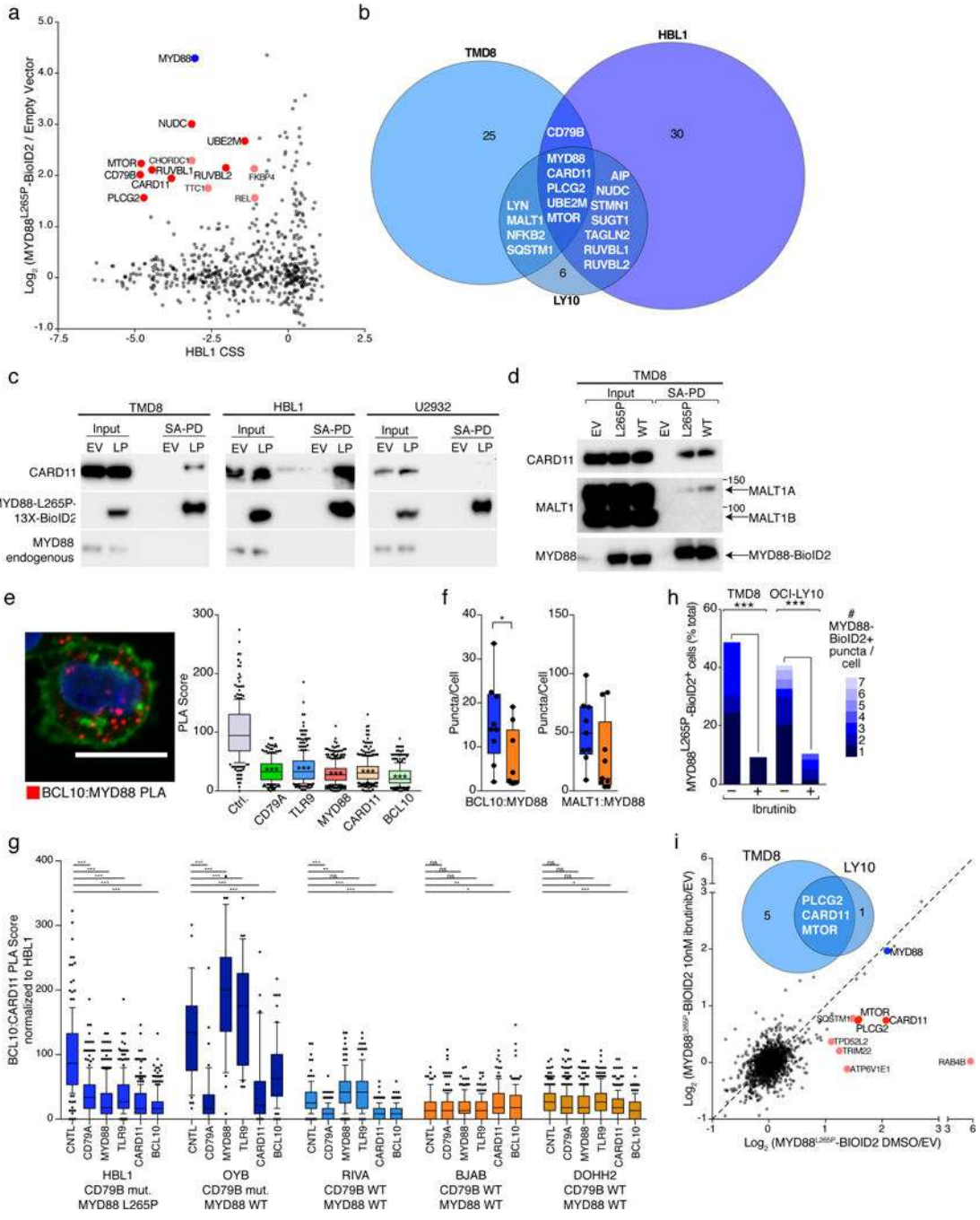

Extended Data Figure 7. The MYD88^{L265P} interactome in ABC DLBCL.

Author Manuscript Author Manuscript Author Manuscript Author Manuscript

Author Manuscript Author Manuscript Author Manuscript Author Manuscript

a, The essential MYD88^{L265P} interactome in HBL1. MYD88^{L265P} -BioID2 interactome from SILAC-based mass spectrometry (y-axis) plotted by the CRISPR screen score (CSS, x-axis). Bait (MYD88) is labeled in blue. Essential interactors are red, with those shared with either TMD8 or OCI-Ly10 labeled in dark red. **b,** Venn diagram of the overlap of MYD88^{L265P} -BioID2 interactors in TMD8, OCI-Ly10 and HBL1 ABC lines. Proteins found in two or more experiments are listed. **c,** Lysates of TMD8, HBL1 and U2932 cells transduced with empty vector or MYD88^{L265P} -BioID2, selected and treated with 50μM biotin for 24 hours. Lysates were prepared and immunoprecipitated with streptavidin before being immunoblotted with CARD11 and MYD88 antibodies. One representative blot is shown for each cell line from n=3 biologically independent experiments (HBL1, TMD8) and n=1 (U2932) **d,** Lysates of TMD8 cells transduced with empty vector, MYD88^{L265P} or wild type (WT) BioID2-fusion proteins, selected and treated with 50μM biotin for 24 hours. Lysates were prepared and immunoprecipitated with streptavidin before being immunoblotted with CARD11, MALT1 or MYD88 antibodies; representative blot; n=3. **e,** Confocal image of a PLA of BCL10 with MYD88. Data pooled from 6 biologically independent replicates of n>200 cells scored per condition. Box plots represent median and 25–75% of data, whiskers display 10–90 percentile; one-way ANOVA with Dunnett's post test. **f,** BCL10:MYD88 and MALT1:MYD88 PLA in ABC (blue, n=9) and GCB (orange, n=9) lines. Box plots represent median and 25–75% of data, whiskers display range; Mann-Whitney unpaired, one-tailed t-test. **g,** BCL10:CARD11 PLA after shRNA knockdown of indicated genes in ABC (blue) and GCB (orange) lines. CD79B and MYD88 mutation status is displayed below each cell line. Data are from 3 fields of cells quantitated from 1 representative experiment of 3 (HBL1), 2 (BJAB, DOHH2) or 1 (OYB, RIVA) biologically independent replicates of n ≥90 cells scored per condition. Box plots represent median and 25–75% of data, whiskers display 10–90 percentile; one-way ANOVA with Dunnett's post test. **h,** ABC lines expressing MYD88^{L265P}-BioID2 were treated with DMSO or 10nM ibrutinib for 24 hours, and the numbers of biotin puncta were quantified from confocal images (representative experiment, n=3). Fisher's exact test, two-sided. **i,** SILAC-based mass spectrometry comparison of MYD88^{L265P}-BioID2 interactome in TMD8 cells treated with DMSO (x-axis) vs. 10nM ibrutinib (y-axis). Proteins reduced upon ibrutinib treatment are shown in red, those similarly decreased in two separate cell lines (Fig. 4A) are labeled in dark red. Bait (MYD88^{L265P}) is labeled in blue. Venn diagraph showing overlap of proteins decreased by ≥30% in OCI-Ly10 cells (Fig. 4a) is shown as an inset.
*p< 0.05, **p<0.01, ***p<0.001. See Statistics and Reproducibility.

Author Manuscript Author Manuscript Author Manuscript Author Manuscript

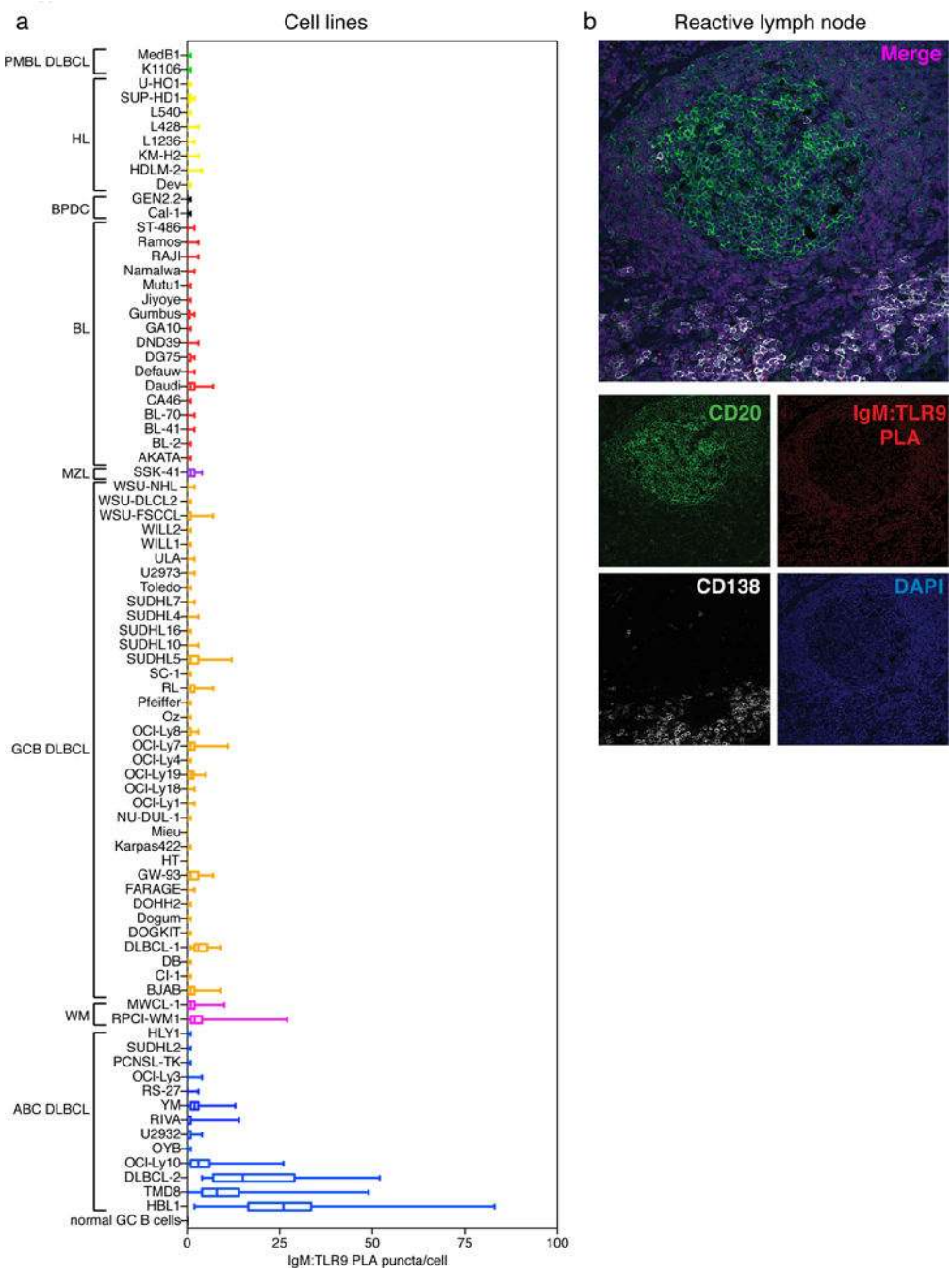

Extended Data Figure 8. IgM:TLR9 PLA identifies ABC samples with chronic active BCR signaling in FFPE TMA.

a, IgM:TLR9 PLA was performed on an FFPE fixed tissue microarray of lymphoma cell lines. PLA puncta were quantified and plotted as the absolute number of spots per cell from at least 2 images of 1 representative experiment from 3 independent TMA replicates. Box plots represent median and 25–75% of data, whiskers display range. Cell lines are divided by putative lymphoma subtype for presentation. PMBL = Primary Mediastinal B cell lymphoma, HL = Hodgkin lymphoma, BPDC = Blastic Plasmacytoid Dendritic Cell neoplasm, BL = Burkitt lymphoma, MZL = Marginal Zone lymphoma, GCB = Germinal

Author Manuscript Author Manuscript Author Manuscript Author Manuscript

Center DLBCL, WM = Waldenström's macroglobulinemia, ABC = Activated B cell-like DLBCL. b, Representative confocal fluorescent image from 3 independent biological samples of a germinal center from a reactive lymph node. IgM:TLR9 PLA is shown in red, ‘CD20 in green, CD138 in white and DAPI in blue.

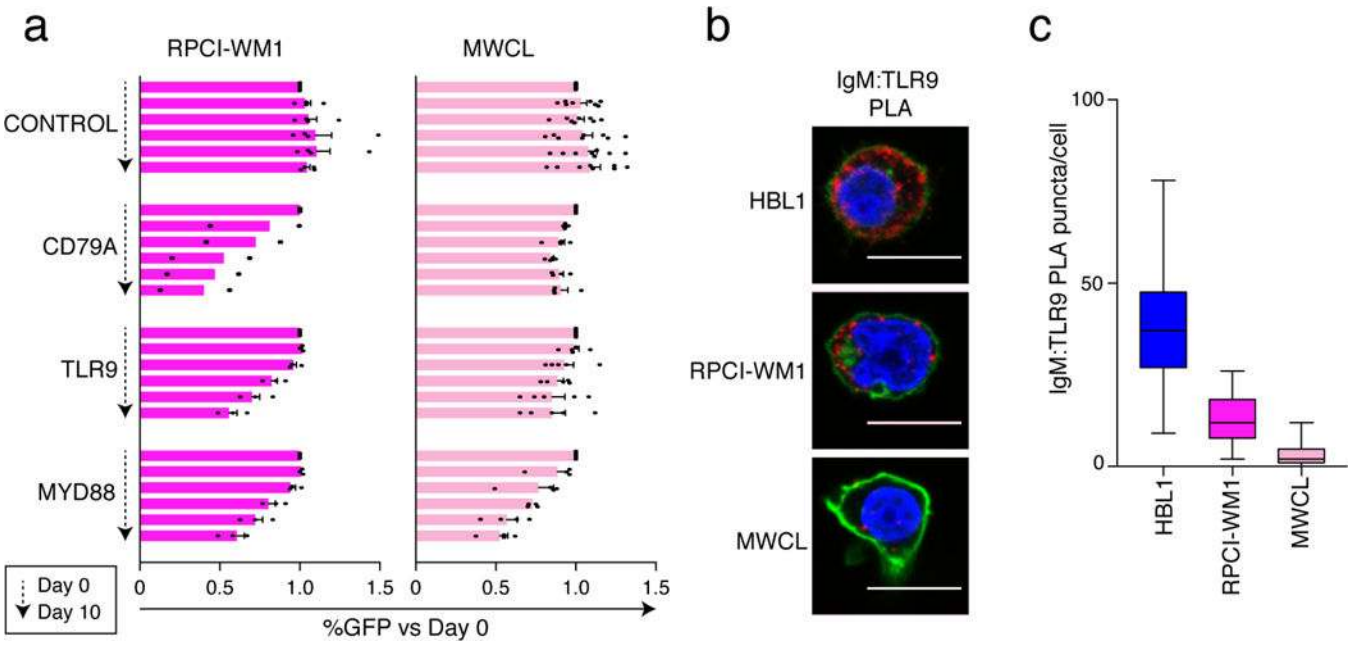

Extended Data Figure 9. Waldenström's macroglobulinemia can utilize the My-T-BCR.

a, shRNA-mediated toxicity of indicated genes in two WM cell lines. Control (SC4), CD79A, TLR9 or MYD88 shRNAs were expressed in tandem with GFP and the relative level of GFP was followed over time by FACS. Mean and SEM are shown of independent biological experiments, n = see Statistics and Reproducibility. b, Confocal images from one of two representative biologically independent experiments of PLA reaction between IgM and TLR9 (red puncta) counterstained with DAPI (blue) and wheat germ agglutinin (green) and c, normalized quantification (PLA Score) of IgM:TLR9. Data were quantitated from n ≥28 cells per condition. Box plots represent median and 25–75% of data, whiskers display range. White scale bar is 10μm.

Supplementary Material

Refer to Web version on PubMed Central for supplementary material.

Acknowledgments

This research was supported by the Intramural Research Program of the NIH, CCR, NCI and by a NCI Strategic Partnering to Evaluate Cancer Signatures (SPECS II) grant (5U01CA157581–05), as well as by Deutsche Krebshilfe (#111399) and Deutsche Forschungsgemeinschaft (SFB1177). DW is a Damon Runyon Fellow (DRG-2208–14). SR is a H2020 Marie Sklodowska-Curie global fellow (#661066). We thank AstraZeneca for AZD2014.

Author Manuscript Author Manuscript Author Manuscript Author Manuscript

References

1. Wilson WH et al. Targeting B cell receptor signaling with ibrutinib in diffuse large B cell lymphoma. Nat Med 21, 922–926, (2015). [PubMed: 26193343]
2. Alizadeh AA et al. Distinct types of diffuse large B-cell lymphoma identified by gene expression profiling. Nature 403, 503–511 (2000). [PubMed: 10676951]
3. Wright G et al. A gene expression-based method to diagnose clinically distinct subgroups of diffuse large B cell lymphoma. Proc Natl Acad Sci U S A 100, 9991–9996 (2003). [PubMed: 12900505]
4. Young RM et al. Survival of human lymphoma cells requires B-cell receptor engagement by self-antigens. Proc Natl Acad Sci U S A 112, 13447–13454, (2015). [PubMed: 26483459]
5. Davis RE et al. Chronic active B-cell-receptor signalling in diffuse large B-cell lymphoma. Nature 463, 88–92, (2010). [PubMed: 20054396]
6. Lenz G et al. Oncogenic CARD11 mutations in human diffuse large B cell lymphoma. Science 319, 1676–1679 (2008). [PubMed: 18323416]
7. Ngo VN et al. Oncogenically active MYD88 mutations in human lymphoma. Nature 470, 115–119, (2011). [PubMed: 21179087]
8. Hart T et al. High-Resolution CRISPR Screens Reveal Fitness Genes and Genotype-Specific Cancer Liabilities. Cell 163, 1515–1526, (2015). [PubMed: 26627737]
9. Schmitz R et al. Burkitt lymphoma pathogenesis and therapeutic targets from structural and functional genomics. Nature 490, 116–120, (2012). [PubMed: 22885699]
10. Lam KP, Kuhn R & Rajewsky K In vivo ablation of surface immunoglobulin on mature B cells by inducible gene targeting results in rapid cell death. Cell 90, 1073–1083 (1997). [PubMed: 9323135]
11. Saitoh S & Miyake K Regulatory molecules required for nucleotide-sensing Toll-like receptors. Immunol Rev 227, 32–43, (2009). [PubMed: 19120473]
12. Schmitz R et al. Genetics and Pathogenesis of Diffuse Large B-Cell Lymphoma. N Engl J Med 378, 1396–1407 (2018). [PubMed: 29641966]
13. Kim DI et al. An improved smaller biotin ligase for BioID proximity labeling. Mol Biol Cell 27, 1188–1196, (2016). [PubMed: 26912792]
14. Soderberg O et al. Characterizing proteins and their interactions in cells and tissues using the in situ proximity ligation assay. Methods 45, 227–232, (2008). [PubMed: 18620061]
15. Sancak Y et al. Ragulator-Rag complex targets mTORC1 to the lysosomal surface and is necessary for its activation by amino acids. Cell 141, 290–303, (2010). [PubMed: 20381137]
16. Zoncu R et al. mTORC1 senses lysosomal amino acids through an inside-out mechanism that requires the vacuolar H(+)-ATPase. Science 334, 678–683, (2011). [PubMed: 22053050]
17. Mathews Griner LA et al. High-throughput combinatorial screening identifies drugs that cooperate with ibrutinib to kill activated B-cell-like diffuse large B-cell lymphoma cells. Proc Natl Acad Sci U S A 111, 2349–2354, (2014). [PubMed: 24469833]
18. Ezell SA et al. Synergistic induction of apoptosis by combination of BTK and dual mTORC1/2 inhibitors in diffuse large B cell lymphoma. Oncotarget 5, 4990–5001, (2014). [PubMed: 24970801]
19. Grommes C et al. Ibrutinib Unmasks Critical Role of Bruton Tyrosine Kinase in Primary CNS Lymphoma. Cancer Discov 7, 1018–1029, (2017). [PubMed: 28619981]
20. Lionakis MS et al. Inhibition of B Cell Receptor Signaling by Ibrutinib in Primary CNS Lymphoma. Cancer Cell 31, 833–843 e835, (2017). [PubMed: 28552327]
21. Nakamura T et al. Recurrent mutations of CD79B and MYD88 are the hallmark of primary central nervous system lymphomas. Neuropathol Appl Neurobiol, (2015).
22. Treon SP et al. Ibrutinib in previously treated Waldenstrom's macroglobulinemia. N Engl J Med 372, 1430–1440, (2015). [PubMed: 25853747]
23. Treon SP et al. MYD88 L265P somatic mutation in Waldenstrom's macroglobulinemia. N Engl J Med 367, 826–833, (2012). [PubMed: 22931316]
24. Brummelkamp TR, Bernards R & Agami R Stable suppression of tumorigenicity by virus-mediated RNA interference. Cancer Cell 2, 243–247 (2002). [PubMed: 12242156]

Author Manuscript Author Manuscript Author Manuscript Author Manuscript

25. Ngo VN et al. A loss-of-function RNA interference screen for molecular targets in cancer. Nature 441, 106–110 (2006). [PubMed: 16572121]

26. Doench JG et al. Optimized sgRNA design to maximize activity and minimize off-target effects of CRISPR-Cas9. Nat Biotechnol 34, 184–191, 10.1038/nbt.3437 (2016). [PubMed: 26780180]

27. Shalem O et al. Genome-scale CRISPR-Cas9 knockout screening in human cells. Science 343, 84–87, 10.1126/science.1247005 (2014). [PubMed: 24336571]

28. Wang T et al. Identification and characterization of essential genes in the human genome. Science 350, 1096–1101, 10.1126/science.aac7041 (2015). [PubMed: 26472758]

29. Wright GW & Simon RM A random variance model for detection of differential gene expression in small microarray experiments. Bioinformatics 19, 2448–2455 (2003). [PubMed: 14668230]

30. Hafner M, Niepel M, Chung M & Sorger PK Growth rate inhibition metrics correct for confounders in measuring sensitivity to cancer drugs. Nat Methods 13, 521–527, 10.1038/nmeth.3853 (2016). [PubMed: 27135972]

31. Mathews Griner LA et al. High-throughput combinatorial screening identifies drugs that cooperate with ibrutinib to kill activated B-cell-like diffuse large B-cell lymphoma cells. Proc Natl Acad Sci U S A 111, 2349–2354, 10.1073/pnas.1311846111 (2014). [PubMed: 24469833]

32. Ceribelli M et al. Blockade of oncogenic IkappaB kinase activity in diffuse large B-cell lymphoma by bromodomain and extraterminal domain protein inhibitors. Proc Natl Acad Sci U S A 111, 11365–11370, 10.1073/pnas.1411701111 (2014). [PubMed: 25049379]

33. Lenz G et al. Molecular subtypes of diffuse large B-cell lymphoma arise by distinct genetic pathways. Proc Natl Acad Sci U S A 105, 13520–13525, doi:0804295105[pii]10.1073/pnas.0804295105 (2008). [PubMed: 18765795]

34. Lam LT et al. Small molecule inhibitors of IkappaB kinase are selectively toxic for subgroups of diffuse large B-cell lymphoma defined by gene expression profiling. Clin Cancer Res 11, 28–40, doi:11/1/28[pii] (2005). [PubMed: 15671525]

35. Ngo VN et al. Oncogenically active MYD88 mutations in human lymphoma. Nature 470, 115–119, doi:nature09671[pii]10.1038/nature09671 (2011). [PubMed: 21179087]

36. Schindelin J et al. Fiji: an open-source platform for biological-image analysis. Nat Methods 9, 676–682, 10.1038/nmeth.2019 (2012). [PubMed: 22743772]

37. Allalou A & Wahlby C BlobFinder, a tool for fluorescence microscopy image cytometry. Comput Methods Programs Biomed 94, 58–65, 10.1016/j.cmpb.2008.08.006 (2009). [PubMed: 18950895]

38. Hewitt SM The application of tissue microarrays in the validation of microarray results. Methods Enzymol 410, 400–415, 10.1016/S0076-6879(06)10020–8 (2006). [PubMed: 16938563]

39. Oellerich T et al. beta2 integrin-derived signals induce cell survival and proliferation of AML blasts by activating a Syk/STAT signaling axis. Blood 121, 3889–3899, S3881–3866, 10.1182/blood-2012-09-457887 (2013). [PubMed: 23509157]

40. Cox J et al. Andromeda: a peptide search engine integrated into the MaxQuant environment. J Proteome Res 10, 1794–1805, 10.1021/pr101065j (2011). [PubMed: 21254760]

Author Manuscript Author Manuscript Author Manuscript Author Manuscript

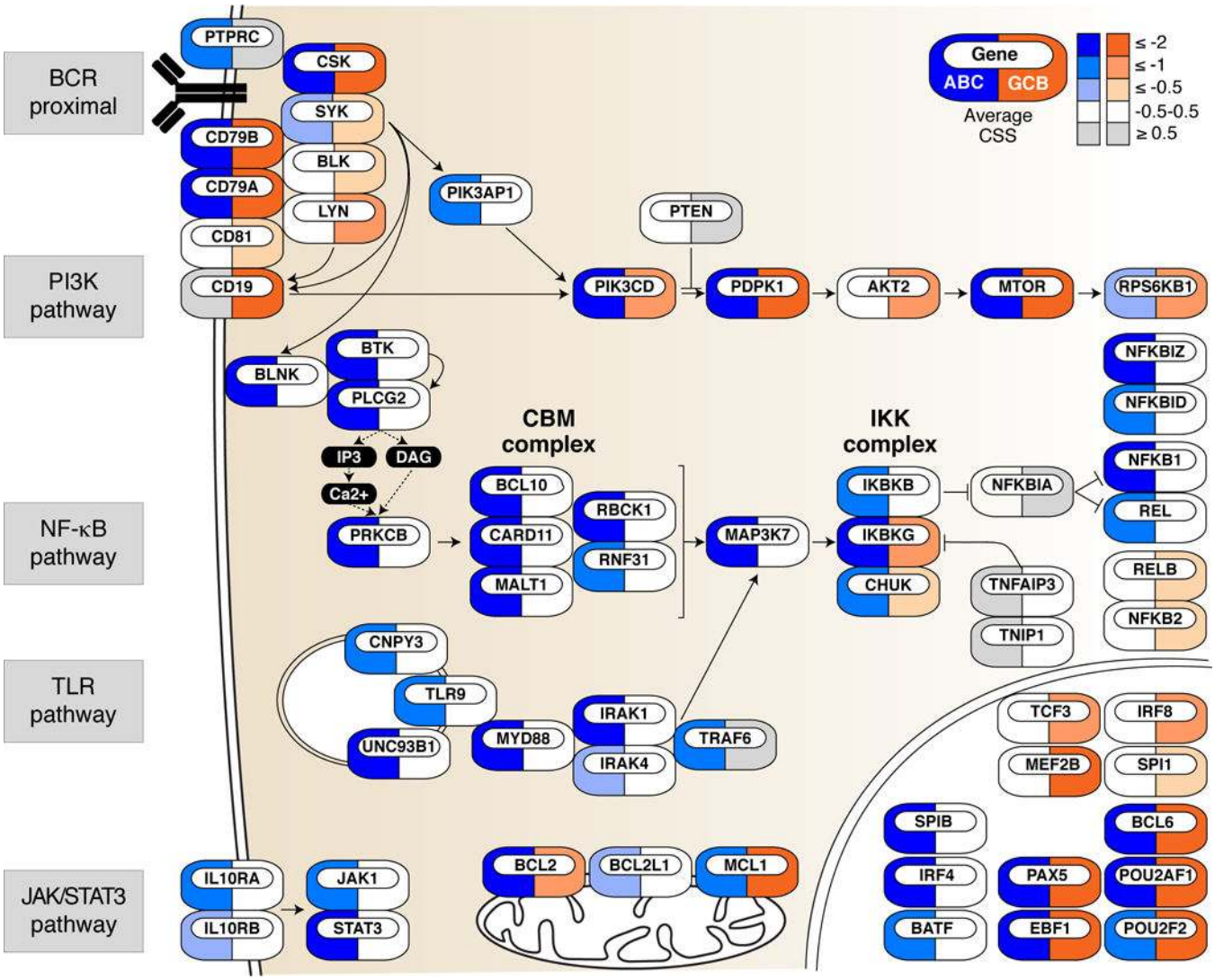

Figure 1. Genes essential for oncogenic signaling in lymphoma.

Icons indicate essential genes from CRISPR screens colored by the average CSS in GCB (orange) or BCR-dependent ABC (blue) DLBCL lines.

Author Manuscript Author Manuscript Author Manuscript Author Manuscript

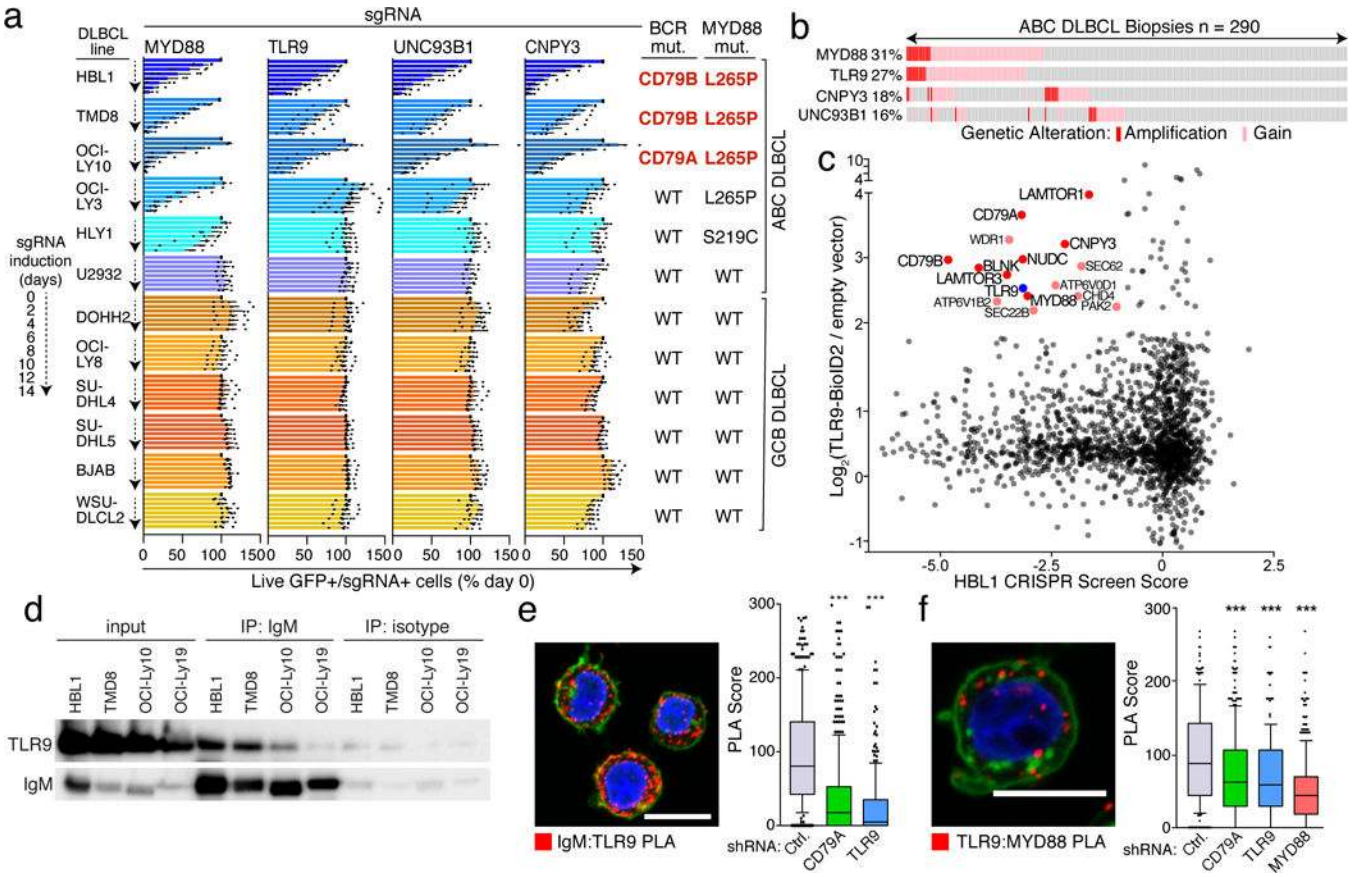

Figure 2. TLR9 couples BCR signaling and mutant MYD88.

a, Toxicity of sgRNAs in DLBCL lines normalized to day 0. **b**, Copy number gain or amplification of indicated genes in ABC biopsies. **c**, TLR9-BioID interactome in HBL1 cells vs. CSS. Blue:bait, red:essential interactors, dark red:essential interactors also in TMD8. **d,** TLR9 co-immunoprecipitates with IgM in ABC lines (HBL1, TMD8, OCI-Ly10). Confocal images of PLAs (red) showing TLR9:IgM (**e**) or TLR9:MYD88 (**f**) interaction in HBL1. DAPI (blue), WGA (green). (right) PLA scores after knockdown of indicated genes. ***p ≤0.001; see Statistics and Reproducibility for additional information.

Author Manuscript Author Manuscript Author Manuscript Author Manuscript

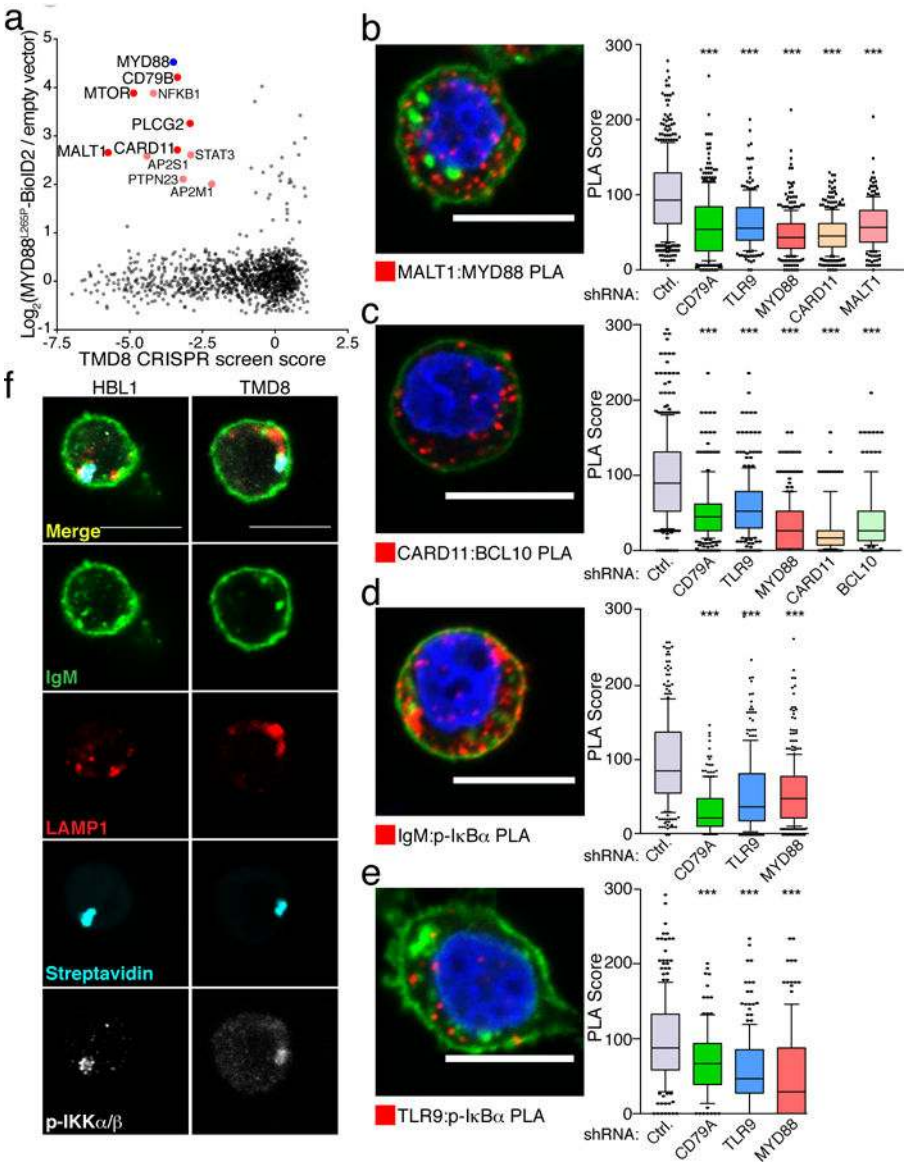

Figure 3. The My-T-BCR supercomplex coordinates NF-κB activation.

a, MYD88^{L265P}-BioID interactome in TMD8 cells vs. CSS. Blue:bait, red:essential interactors, dark red:essential interactors in ≥2 ABC lines. Confocal image of PLAs (red) showing interaction of **b,** MALT1:MYD88; **c,** CARD11:BCL10 **d**, IgM:p-IκBα **e,** TLR9:p-IκBα. DAPI (blue); WGA (green). (right) PLA scores in HBL1 cells after knockdown of indicated genes. **f,** Confocal images of MYD88^{L265P}-BioID-transduced HBL1 or TMD8 cells stained as indicated. ***p ≤0.001; see Statistics and Reproducibility for additional information.

Author Manuscript Author Manuscript Author Manuscript Author Manuscript

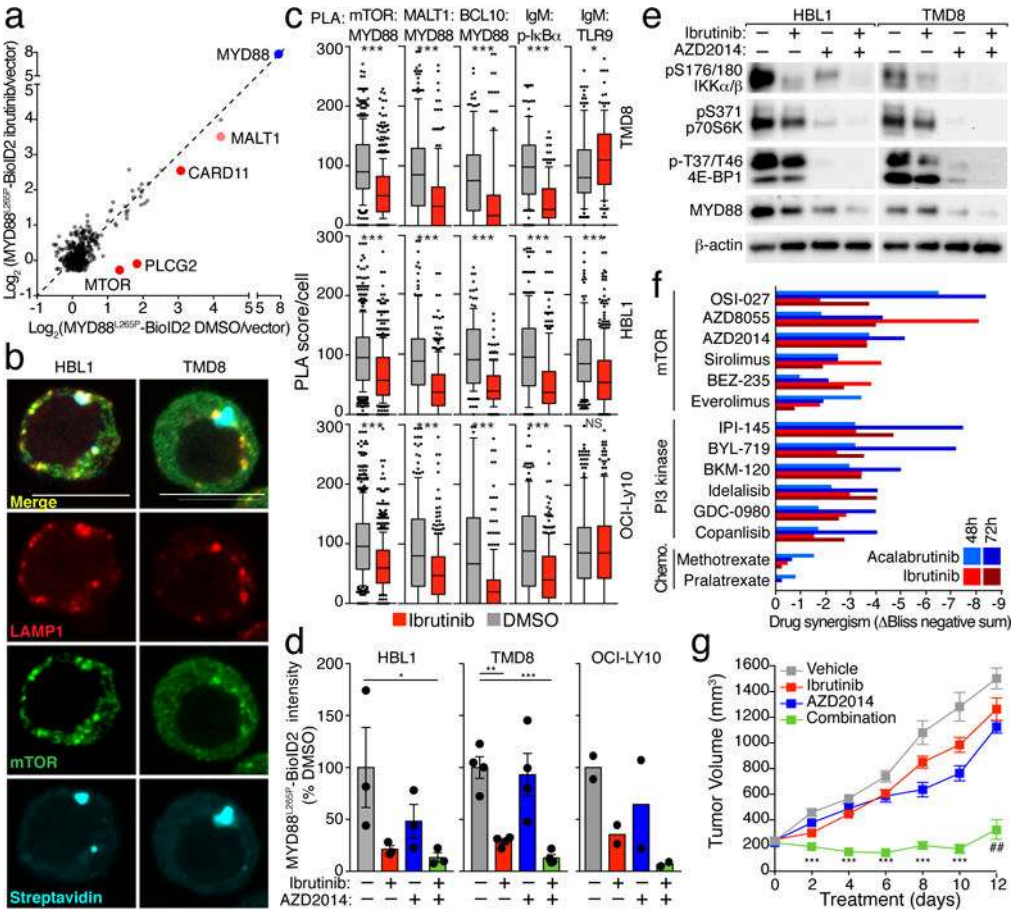

Figure 4. mTOR is an essential component of the My-T-BCR supercomplex.

a, MYD88^{L265P}-BioID interactome in OCI-Ly10 cells treated with ibrutinib (10nM) or DMSO. Red: ibrutinib-sensitive interactions, blue:bait. **b,** Confocal images of mTOR (green), LAMP1 (red) and MYD88^{L265P}-BioID2 (cyan, streptavidin) in ABC cells. **c,** PLA scores for indicated protein interactions in ABC lines treated with ibrutinib or DMSO. **d,** Normalized MYD88^{L265P}-BioID intensity/cell in ABC lines treated as indicated for 24 hours. **e,** Immunoblots using the indicated antibodies of ABC lines treated with indicated drugs for 24 hours. **f,** Synergistic toxicity scores in TMD8 cells treated with ibrutinib or acalabrutinib together with the indicated drugs. **g,** Growth of TMD8 xenografts in NSG mice treated as indicated. ***p ≤0.001, **p ≤0.01, *p ≤0.05; see Statistics and Reproducibility for additional information.

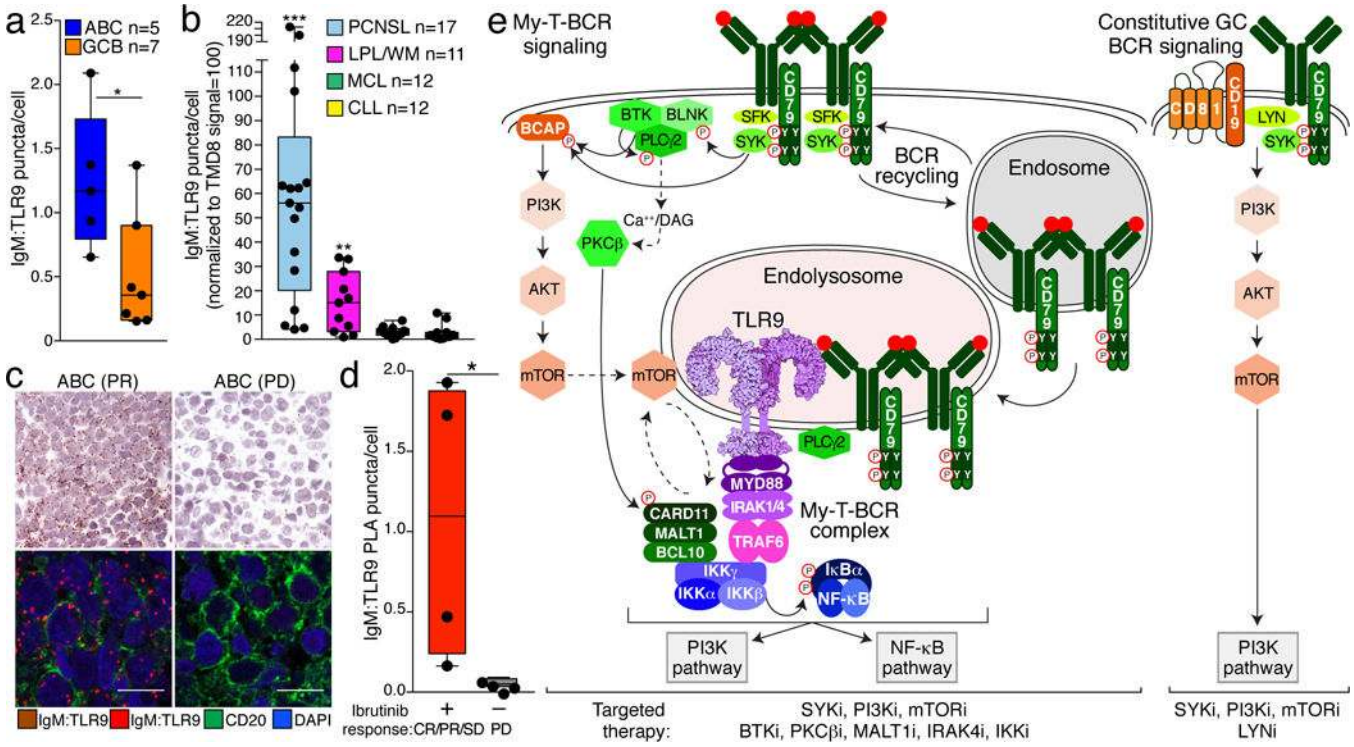

Figure 5. The My-T-BCR complex identifies ibrutinib-responsive lymphomas.

IgM:TLR9 PLA puncta/cell in **a,** GCB and ABC biopsies or **b,** indicated lymphoma biopsies. **c,** Representative IgM:TLR9 PLA images of ABC biopsies. Bright field (top) fluorescence (bottom). PR: partial response, PD: progressive disease. **d,** IgM:TLR9 PLA of biopsies from DLBCL patients treated with ibrutinib. Responders (red; complete response (CR), PR, stable disease (SD)), non-responders (grey; PD). **e,** Models of My-T-BCR signaling and constitutive GC BCR signaling. ***p ≤0.001, **p ≤0.01, *p ≤0.05; see Statistics and Reproducibility for additional information.

Author Manuscript Author Manuscript Author Manuscript Author Manuscript